Title
A SIMULATION MODEL FOR THE PERFORMANCE ANALYSE OF POOF POND SYSTEMS FOR HEATING AND COOLING

Author
Tavana, M.

Publication Date
1980-10-01

LBL-9292 c.2

Lawrence Berkeley Laboratory
UNIVERSITY OF CALIFORNIA

ENERGY & ENVIRONMENT DIVISION

Presented at the American Section/International Solar Energy Society Solar Jubliee, Phoenix, AZ, June 2-6, 1980

A SIMULATION MODEL FOR THE PERFORMANCE ANALYSIS OF ROOF POND SYSTEMS FOR HEATING AND COOLING

Mehdi Tavana, Hashem Akbari, Tom Borgers, and Ronald Kammerud

October 1980

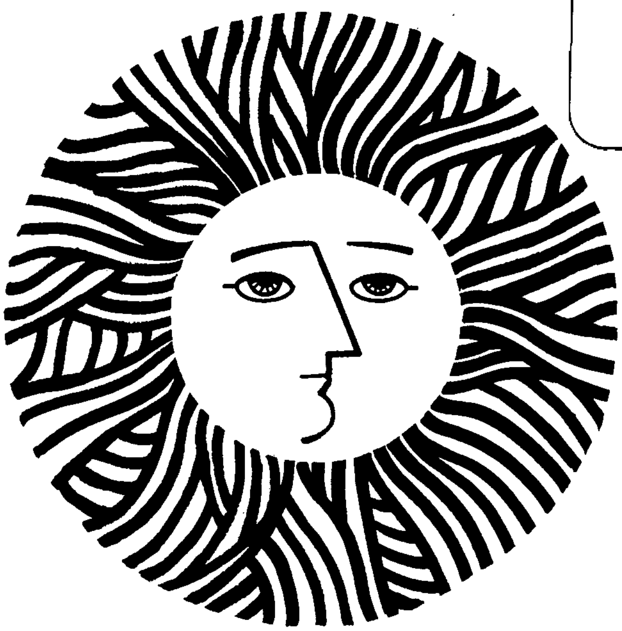

Prepared for the U.S. Department of Energy under Contract W-7405-ENG-48

DISCLAIMER

LBL-9292
October 1980

A SIMULATION MODEL FOR THE PERFORMANCE ANALYSIS OF ROOF POND SYSTEMS FOR HEATING AND COOLING*

M. Tavana, H. Akbari, T. Borgers,† and R. Kammerud
Passive Solar Analysis and Design Group
Lawrence Berkeley Laboratory
University of California
Berkeley, CA 94720

ABSTRACT

A detailed computer model has been developed for simulating the dynamic thermal behavior of roof pond systems. The model is composed of outer movable insulation, an optional evaporative water layer over water bags on steel decking and an inner movable insulation; a movable insulation control strategy which provides near optimum thermal performance is included in the model. An hourly heat balance analysis of the system is performed using theoretical and/or empirical expressions to determine the heat transfer coefficients for each of the different surfaces in the model. The model has been used to study the effect on system thermal performance of (1) the R value of both the top and bottom movable insulations, (2) the depth of pond water, and (3) the depth of the evaporative layer. The model has also been used to investigate the heating and cooling potentials of the roof pond in four different climates.

The model was developed for incorporation into the public domain building energy analysis computer program BLAST.§

---

*This work was supported by the Passive and Hybrid Systems Branch, Systems Development Division, Office of Solar Applications for Buildings, U.S. Department of Energy, under Contract No. W-7405-ENG-48.

†Department of Chemistry, California State University at Humboldt, Arcata, California 95521.

§Building Loads Analysis and System Thermodynamics. BLAST is copyrighted by the Construction Engineering Research Laboratory, U.S. Department of the Army, Champaign, Illinois.

I. INTRODUCTION

The concept of using water on roofs as a moderator of the indoor climate has long been recognized and practiced. Recently investigators have begun to quantify its energy saving potentials [1-10]. In 1967-68 a small-scale prototype was tested in Phoenix, Arizona; it was found that throughout a normal year the room air temperatures could be maintained between 17 and 28^{o}C without supplementary heating or cooling [1-3]. A full-size test house was tested in Atascadero, California during 1973 and 1974. The applicability of the system in the Atascadero climate was proved [5-6]. Data on the performance of a roof pond solar house located on the Campus of New Mexico State University in Las Cruces, New Mexico has also shown that such a system operates well [8] in this climate. Heating season performance of a mobile/modular home which incorporated roof pond with insulated clerestory windows across the roof was tested during 1978-1979 in Los Alamos, New Mexico [9]; this system provided nearly 90% of the heating energy requirements of the structure in the 7800 DD (65^{o}F base) climate of Los Alamos. Clark, et al. [10] developed a computer model which predicted that a substantial reduction in cooling energy requirements is possible even in the more humid regions of the United States if the roof pond is provided with evaporative enhancement. Other studies have shown the advantages of water-flooded roofs for cooling purposes [11-13].

The activities referred to above have demonstrated that roof pond systems have substantial potentials for reducing auxiliary energy consumption in climates requiring both heating and cooling. In order to provide an improved engineering basis for designing and operating a roof pond system, it is desirable to have a general simulation capability which permits examination of the performance of buildings utilizing roof ponds in order to study the effect of various parameters in different climates. The purpose of the work reported here was to develop a public domain simulation model of sufficient flexibility to (1) permit rapid evaluation of heating and cooling potentials of roof pond systems, and (2) to optimize parameters such as insulation thicknesses and pond and evaporative layer depths. This model will be incorporated into the public domain building energy analysis computer program BLAST.

II. MODEL

The physical elements represented in this model are shown in Fig. 1; starting from the top, they include (1) an optically opaque movable top insulation which controls the coupling of the pond to the external environment; (2) an air gap between the insulation and the pond; (3) an optional layer of water which can provide evaporative enhancement of the system; (4) a plastic membrane encasing the water of the pond; (5) pond water; (6) a steel support deck; (7) an air gap between the deck and the bottom insulation; and (8) a movable bottom insulation which controls the coupling of the pond to the conditioned space. During the heating season, the top insulation panels are opened during the day so that solar energy may be collected and stored in the water and transferred to the conditioned space. Night losses are reduced by closing the upper insulation; heat may continue to flow into the room from the warm water by leaving the bottom insulation open. In more severe conditions the lower insulation is also operated to further reduce the heat losses to the outside air.

During the cooling season, the top insulation is closed during the day to prevent solar gains and is opened at night to permit radiative, and convective heat losses. Cooling is achieved by flooding the encased pond with water. Both the upper and lower insulation may be independently positioned to control the degree of cooling.

To the authors knowledge, no roof pond systems we recognize incorporating the bottom insulation have been built. We recognize the complications associated with movable insulation near the ceiling in the occupied space, however, there are potential benefits. The panels could provide a degree of control over the interaction of the thermally massive roof pond with the occupied space, affecting both convective coupling and, perhaps more importantly, radiative coupling. In the roof pond model described here, the addition of lower insulation is little different than increasing the thermal resistance of the top insulation. It could, however, be beneficial in reducing the auxiliary cooling load when cloudy nights would not allow the pond water to cool down sufficiently during the cooling season. In addition, in extremely severe conditions during the heating season, it could be utilized to reduce the heat losses to the outside air; losses due to infiltration of air through the air gap between the top insulation panels and the pond can not be reduced by increasing the amount of top insulation. A meaningful assessment of the influence of the bottom insulation on the energy consumption and/or comfort levels of the building can be carried out after the model has been incorporated into a building energy analysis program which allows room temperatures to float and which calculates radiant temperatures within the occupied space.

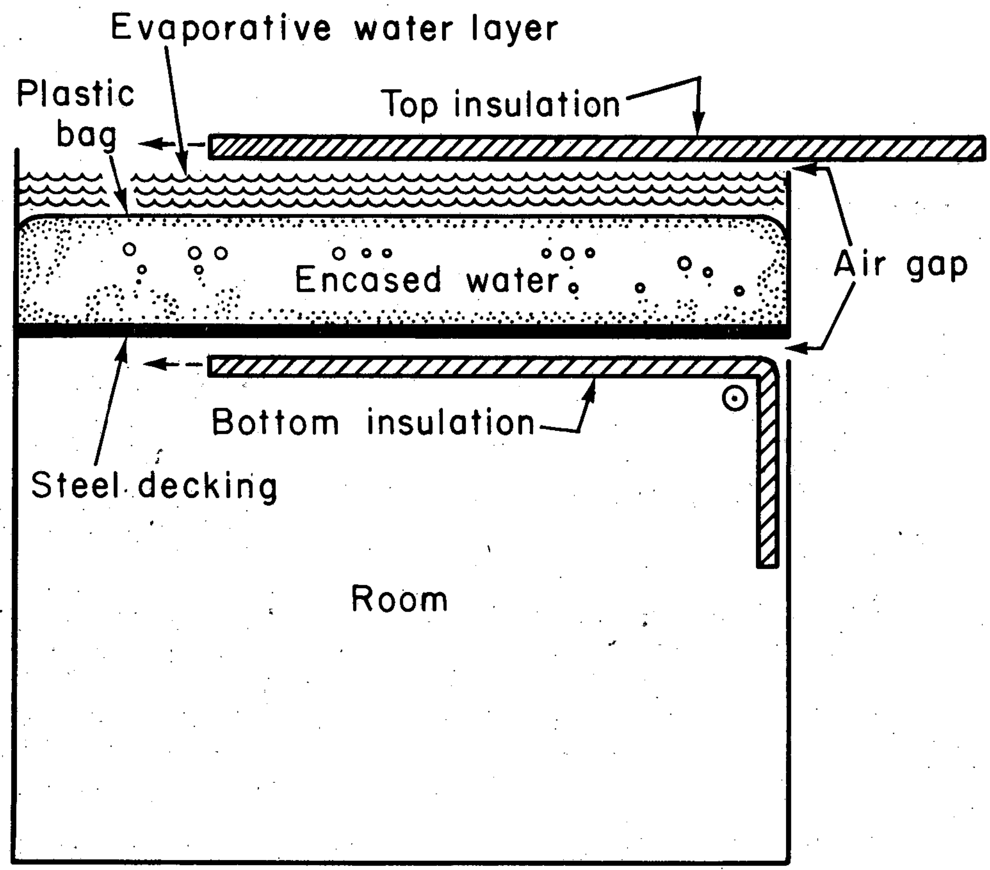

SCHEMATIC OF ROOF POND MODEL COMPONENTS

XBL 803-6688

FIGURE 1.

The one-dimensional heat transfer model described here makes extensive use of empirical relations found in the literature, and a number of simplifying assumptions. For clarity, a detailed description of the model is presented in three sections below: components; environmental conditions and properties; and the computational procedure.

II.1 Components

The roof pond system is defined as the collection of elements which are bounded by the outside air and the room air; the outer top insulation surface (if present) is one boundary and the room side of the lower insulation (if present) is the other. The model assumes that all heat flows through the structure elements of the system are one-dimensional. The model considers three categories of heat exchange; (1) the interaction of the system with the outside world, (2) the coupling of the system to the room, and (3) the internal thermal exchange between the elements of the system itself.

II.1.1 Interaction of the System with the External Environment

The interaction of the system with the environment may consist of some or all of the following: solar collection, infrared radiative exchange with the sky, and heat transfer by means of convection-conduction and evaporation between the system and the ambient air.

II.1.1.1 Solar Collection

When solar radiation with a horizontal surface intensity H_0 is incident on the system, it strikes either the outer insulation or the pond itself. If the insulation is opaque and highly reflective with absorptance α, then only αH_0 will be absorbed by the surface, the remainder being totally reflected. Should it strike the uncovered plastic bag encasing the water of the pond, the incident solar radiation is partly reflected into the air and the remainder is partly absorbed in the plastic layer, partly absorbed in the pond water, and the remainder is assumed to be absorbed by the steel deck.

The absorption of the radiation as it passes through a medium is a function of the absorption (or extinction) coefficient of that medium. The intersity of solar radiation at any optical depth X is given by

$$H(X) = (HO)\, e^{-\frac{\mu}{m} X} , \qquad (1)$$

where $H(X)$ = intensity of radiation reaching an optical depth X, $kJ \cdot m^{-2}hr^{-1}$

$H(0)$ = intensity of radiation entering the medium, $kJ \cdot m^{-2}hr^{-1}$

μ = absorption coefficient of the medium, Cm^{-1}

X = path length of radiation through the medium, Cm.

For the absorption of solar radiation in plastic, a single overall absorption coefficient, μ, is used. For water, different wavelengths differ widely in their absorption coefficients.

It has been determined that five wavelength segmens are adequate to describe the attenuation of solar radiation as it passes through the water [14]. This selective absorption is described by a slightly modified expression from Ref. [15]:

$$H(X) = H(0) \sum_{n=1}^{5} \mu_n e^{-\mu_n X}$$

with

$$\begin{aligned} \eta_1 &= 0.237 & \mu_1 &= 3.2 \times 10^{-4}\ cm^{-1} \\ \eta_2 &= 0.193 & \mu_2 &= 4.5 \times 10^{-3} \\ \eta_3 &= 0.167 & \mu_3 &= 3.0 \times 10^{-2} \\ \eta_4 &= 0.179 & \mu_4 &= 0.35 \\ \eta_5 &= 0.224 & \mu_5 &= 2.6 \end{aligned}$$

In the absence of the evaporative layer, the following expressions are obtained for the total radiation absorbed by the plastic membrane (including the effects of multiple reflection), the encased water, and the steel plate, respectively:

$$E_p = (1 - \rho_{ap})H_0 \frac{(1 - g_p)(1 + \rho_{pw} g_p)}{1 - \rho_{ap}\rho_{pw} g_p^2} \tag{3}$$

$$E_W = (1 - \rho_{ap})H_0 \frac{(1 - \rho_{pw}) g_p}{1 - \rho_{ap}\rho_{pw} g_p^2} \sum_{n=1}^{5} \eta_n (1 - g_{wn}) \tag{4}$$

$$E_S = (1 - \rho_{ap})H_0 \frac{(1 - \rho_{pw}) g_p}{1 - \rho_{ap}\rho_{pw} g_p^2} \sum_{n=1}^{5} \eta_n g_{wn} \tag{5}$$

where

$$g_p = e^{-\mu_p d_{pc}} \tag{6}$$

$$g_{wn} = e^{-\mu_n d_{wc}} \tag{7}$$

E_p = total solar radiation absorbed by the plastic membrane, $kJ \cdot m^{-2}hr^{-1}$
E_W = total solar radiation absorbed by the pond water, $kJ \cdot m^{-2}hr^{-1}$
E_S = total solar radiation absorbed by the steel decking, $kJ \cdot m^{-2}hr^{-1}$
ρ_{ap} = reflectance at the air-plastic interface
ρ_{pw} = reflectance at the plastic-water interface
d_{pc} = path length of radiation through the plastic membrane, cm
μ_p = overall absorption coefficient of plastic, cm^{-1}
d_{wc} = path length of radiation through pond water, cm.

The reflectance at the interface of the two media is calculated from the angle of incidence and the refraction indices of the two media by using Fresnel's relationship and Snell's law.

If the evaporative layer is present the energies absorbed in the evaporative layer, including the effects of multiple reflection, plastic member, encased water, and steel plate, are given (respectively) by:

$$E_F = (1 - \rho_{aw})H_0 \sum_{n=1}^{5} \eta_n \frac{(1 - g_{fn})(1 + \rho_{pw} g_{fn})}{1 - \rho_{aw}\rho_{pw} g_{fn}^2} \tag{8}$$

$$E_P = (1 - g_p)(1 - \rho_{pw})(1 - \rho_{aw})H_0 \sum_{n=1}^{5} \eta_n \frac{g_{fn}}{1 - \rho_{aw}\rho_{pw} g_{fn}^2} \tag{9}$$

$$E_W = (1 - \rho_{pw})(1 - \rho_{aw}) g_p H_0 \sum_{n=1}^{5} \eta_n \frac{g_{fn}(1 - g_{wn})}{1 - \rho_{aw}\rho_{pw} g_{fn}^2} \tag{10}$$

$$E_S = (1 - \rho_{pw})(1 - \rho_{aw}) g_p H_0 \sum_{n=1}^{5} \eta_n \frac{g_{fn} g_{wn}}{1 - \rho_{aw}\rho_{pw} g_{fn}^2} \tag{11}$$

where

$$g_{fn} = e^{-\mu_n d_{fc}} \tag{12}$$

E_F = Total solar radiation absorbed by the evaporative layer, $kJ\text{-}m^{-2}hr^{-1}$

ρ_{aw} = Reflectance at the air-water interface

d_{fc} = Path length of radiation through evaporative layer, cm

Losses due to multiple reflections are not expected to be large. Multiple reflections are considered only within the first top layer of the roof pond system, namely the plastic or evaporative layer. These losses are even less significant for lower layers since a greater portion of the reflected energy will be absorbed by the roof pond layers. For a detailed derivation of these relations refer to Appendix I.

II.1.1.2 Radiation Exchange With The Sky

The radiative energy exchange between the system and the sky is given by:

$$Q_r = \varepsilon_i \sigma (T_i^4 - T_{sky}^4) \tag{13}$$

where

Q_r = Radiative heat exchange rate between the system outer surface and the sky, $kJ\text{-}m^{-2}$

ε_i = Emissivity of the surface exposed to the sky

σ = Stefan-Boltzman constant, $kJ\text{-}m^{-2}hr^{-1}{}^{o}K^{-4}$

T_i = Temperature of the surface exposed to the sky; this may be top insulation, plastic membrane, or evaporative layer surface, ^{o}K

T_{sky} = Effective radiative sky temperature, ^{o}K

The sky is assumed to be a black body with an effective temperature which is estimated by

$$T_{sky} = \varepsilon_{se}^{1/4} T_a \tag{14}$$

where T_a is the dry bulb ambient temperature in ^oK and the effective sky emissivity, ε_{se}, is related to the clear sky emissivity, ε_{sc}, by assuming a linear cloud cover dependence

$$\varepsilon_{se} = \varepsilon_{sc} + (1 - \varepsilon_{sc})C \tag{15}$$

with C = cloud cover in tenths, (0 to 1). Equation (15) is an over-simplification which suggests zero net radiation exchange for a cloud cover of 1. It tends to underestimate the infared radiation losses to the sky for cloudy days. The clear sky emissivity is obtained from [18]

$$\varepsilon_{sc} = 0.605 + 0.048\sqrt{e_a} \tag{16}$$

where

e_a = Atmospheric water-vapor pressure, millibar.

II.1.1.3 Convection-Conduction and Evaporation Heat Exchange

The combined convection-conduction heat transfer coefficient for the non-flooded case between the ambient and the plastic membrane or outer insulation surface is obtained from Ref. [19]:

$$h_C = 20.5 + 3.9W \tag{17}$$

where

h_c = Convection-conduction heat transfer coefficient $kJ \cdot m^{-2} hr^{-1} {}^oC^{-1}$

W = Wind speed, $km\text{-}hr^{-1}$

The convective-conductive heat transfer is then

$$Q_C = (h_C(T_i - T_a) \tag{18}$$

When the evaporative layer is present, the convective-conductive heat transfer between the surface and the ambient is given by [20,21]

$$Q_C = 8.517 \times 10^{\ 3}(T_f - T_a)P\left[157.9W + 692(T_{fv} - T_{av})^{1/3}\right] \tag{19}$$

where $$T_{fv} = T_f/(1 - 0.378 e_f P^{-1}) \tag{20}$$

$$T_{av} = T_a/(1 - 0.378 e_a P^{-1}) \tag{21}$$

Q_C = Convection-conduction heat transfer rate, $kJ\text{-}m^{-2}hr^{-1}$

T_f = Temperature of the evaporative layer, ^oK

e_f = Saturated water vapor pressure at temperature T_f, atm

P = Atmospheric pressure, atm

Note that in Eq. (21) T_a is in ^oK and e_a in atm. The heat loss due to evaporation is given by [21];

$$Q_e = 14.158 \left[157.9W + 692(T_{fv} - T_{av})^{1/3}\right](E_f - e_a) \qquad (22)$$

In Eq. (22) the term 157.9W represents the forced convection and the term $692(T_{fv} - T_{av})^{1/3}$ accounts for the free convection effects. Jirka, et al., [22] recommends a coefficient of 219.7 instead of 157.9 for wind velocity. When using Eq. (22), if $e_f < e_a$, e_f is set equal to e_a, and if $T_f < T_a$, the values of T_{fv} and T_{av} are taken to be the same. In the case where the evaporative layer is covered with top insulation, no evaporative cooling is considered by the model.

Equation (19) is obtained from Eq. (22) based on the analogy between heat and mass transfer processes. Thus if $T_{fv} < T_{av}$, the difference $T_{fv} - T_{av}$ is set equal to zero in Eq. (19).

The volumetric flow rate of make-up water is

$$V_w = 4.1 \times 10^{-4} Q_e \qquad (23)$$

and the heat required to bring make-up water temperature from T_m to T_f is

$$Q_w = 1.7165 \times 10^{-3} Q_e(T_f - T_m) \qquad (24)$$

The units of V_w and Q_w are liter $m^{-2}hr^{-1}$ and $kJ\text{-}m^{-2}hr^{-1}$ respectively.

II.1.2 Interaction with the Occupied Space

The heat exchange between the system and the room includes the effects of radiation, conduction, and convection. The radiative exchange between either the steel decking or the bottom surface of the inner insulation panel and the room, both assumed to be black surfaces, is given by

$$Q_{rm} = (T_j^4 - T_r^4) \qquad (25)$$

where

Q_{rm} = Radiative heat exchange rate between the steel on the bottom of the inner insulation and the room, kJ-m^{-2}hr^{-1}

T_j = Temperature of the steel or bottom surface of the inner insulation, ^oK

T_r = Room air temperature, ^oK

It is apparent that this approximation should be altered to recognize more realistic conditions. For example, the room temperture used here does not take into account wall surface temperature differences, radiative view factors, the emissivities of each of the different surfaces, or the fact that usually the mean air temperature differs from the mean radiative temperature.

The convective-conductive heat transfer coefficient between the system and the room is calculated from the Nusselt number [23]:

$$Nu = C(Ra)^m \tag{26}$$

where

Nu = Nusselt number h_c L/K, dimensionless

L = Characteristic length, m

K = Thermal Conductivity, kJ-m^{-1}hr^{-1} $^oC^{-1}$

Ra = Rayleigh number Gr Pr, dimensionless

Gr = Grashof number $\beta\rho^2 \Delta T L^3 g/\mu^2$, dimensionless

β = Volumetric expansion coefficient, $^oC^{-1}$

ρ = Density, kg-m^{-3}

ΔT = Temperature difference, ^oC

g = Gravity acceleration, m hr^{-2}

μ = Viscosity, kg-m^{-1}hr^{-1}

Pr = Prandtl number, $C_p\mu/K$, dimensionless

C_p = Heat capacity, kJ-kg^{-1} $^oC^{-1}$

If heat is entering the room from the system, C = 0.58 and m = 0.2. Should heat flow from the room to the system the values of C and m are:

$$C = 0.54, \quad m = 0.25 \quad \text{for} \quad Ra < 8\times10^6$$

or

$$C = 0.15, \quad m = 0.333 \quad \text{for} \quad Ra > 8\times10^6$$

The characteristic length used in computing Rayleigh number, Ra, is an average length of the steel plate or the insulation. Minimum heat transfer coefficients of 4.5 $kJ\text{-}m^{-2}hr^{-1}\,{}^{o}C^{-1}$ for downward heat flow and 15.5 $kJ\text{-}m^{2}hr^{o}C^{-1}$ for upward heat flow are determined by considering both the boundary layer thickness and the thermal conductivity of air [24].

II.1.3 Internal Interaction

Thermal exchange between the elements of the system is based on the assumption that the plastic membrane and the steel decking have negligible thermal capacity. Heat flow through the top and bottom insulation is assumed to include only conduction. Heat flow across the air gaps is composed of radiation and conduction-convection. For radiative heat exchange across the gap a mean radiative temperature equal to the average of the temperatures of the two surfaces in contact with the air gap is used. For conduction-convection across the air gaps, the Nusselt number [25]

$$Nu = 0.069(Gr)^{0.333}(Pr)^{0.407} \qquad (27)$$

is used for upward heat flow whenever the estimated heat transfer coefficient is greater than that of pure conduction. If the estimated heat transfer coefficient is less than that of pure conduction, or if heat is flowing downward, heat transfer is considered to be by conduction only. The characteristic length used in Eq. (27) is the air gap thickness. At present, the model does not consider outside air infiltration to the upper air gap.

The Heat transfer coefficient between the plastic or the steel and water is estimated by Eq. (26), where the characteristic length is taken to be an average length of the water bag. A minimum heat transfer coefficient of 50 $kJ\text{-}m^{-2}hr^{-1}\,{}^{o}C^{-1}$ for downward heat flow and 300 $kJ\text{-}m^{-2}hr^{-1}\,{}^{o}C^{-1}$ for upward flow is determined by considering both the boundary layer thickness and the thermal conductivity of water.

II.2 ENVIRONMENTAL CONDITIONS AND PROPERTIES

II.2.1 Environmental Conditions

The environmental conditions which govern the performance of the roof pond are insolation, ambient temperature, relative humidity, wind velocity, and cloud cover. Though the code easily can be amended to accommodate hourly meteorological data, for the simulations reported here, monthly average values of the above parameters were used to generate hourly data for a representative average day for each month. Monthly average daily total solar radiation data on a horizontal surface were taken from Refs. [16] and [26] to generate hourly horizontal insolation values following the procedure of Liu and Jordan [27] with supporting relationships from [17]. No distinction is made between direct and diffuse radiation and the total value is treated as if it were all direct.

The average monthly dry bulb maximum and minimum temperatures taken from Refs. [16] and [28] were used to generate a 24-hourly profile for each month. The hourly temperatures are given by

$$T_I = T_{max} - C_I(T_{max} - T_{min}) \quad , \qquad (28)$$

where

T_I = Temperature at hour I, °C

T_{max} = Monthly average maximum temperature, °C

T_{min} = Monthly average minimum temperature, °C

The values of C_I for each hour I, taken from BLAST, are given in Table I.

TABLE 1

Hour	C_I	Hour	C_I
1	.82	13	.23
2	.87	14	.11
3	.92	15	.03
4	.96	16	0.0
5	.99	17	.03
6	1.0	18	.10
7	.98	19	.21
8	.93	20	.34
9	.84	21	.47
10	.71	22	.58
11	.56	23	.68
12	.39	24	.76

Monthly mean values are commonly reported in the literature for four different hours during the day. Maximum and minimum relative humidities for the day were assumed to be the highest and lowest of the monthly mean values. It was assumed that the maximum and minimum relative humidities are coincident with the minimum and maximum dry bulb temperatures, respectively. These values were used to compute maximum and minimum wet bulb temperatures according to algorithms from Ref. [29]. The 24 hourly wet bulb temperature profile was then generated by the same procedure as used for the dry bulb temperature.

II.2.2 Properties

The physical properties of air used in the equations of heat transfer are relatively constant over the temperature range of interest. Therefore, with the exception of the coefficient of expansion, the properties were approximated using the values at $300^{o}K$. The coefficient of expansion of air was taken equal to 1/(absolute temperature of air).

All physical properties of water except the heat capacity were calculated as functions of temperature. The equations used to estimate the water properties are given in Appendix II.

II.3 Calculation Procedure

The top and bottom insulations are positioned to maximize heat gain during the heating season, and heat loss during the cooling months which is accomplished by an insulation control strategy heat loss described in the next section. The dynamic behavior of the system is simulated by performing steady state thermal balance calculations at each time step; writing heat balance equations for each element of the system considering all relevant mechanisms of heat transfer, namely radiation, conduction, convection, and evaporation. During each time step, iterative procedures are used to calculate the temperatures of the outer surface of the top insulation (if present), the plastic, and the steel decking until successive values are within $0.1^{o}C$. Simultaneously, the heat transfer coefficients between the elements of the system are evaluated. Since the thermal capacities of these three elements are assumed negligably small, all absorbed energy is immediately dissipated. After all heat flux components of the system are computed, the new temperatures of the encased water and the evaporative layer (if present) are determined. Some of the heat transfer terms in the heat balance equations of water and evaporative layer are highly temperature-sensitive; these terms were therefore evaluated over shorter time periods, while other less sensitive components were assumed constant over the hour interval.

It was found that, during each hourly time step, three time sub-steps are adequate to determine the temperature of the encased water, and three steps to determine the evaporative layer temperature. Whenever the top insulation covers the roof pond assembly, the additional steps taken to determine the temperature of the evaporative layer are unnecessary. The detailed calculation procedure is presented in Appendix III.

The daily simulation begins with estimates of the temperature for each element of the system model. The calculation, (with the conditions at the end of one day providing initial conditions for the following identical day), is repeated until the system reaches a periodic steady state.

III. SIMULATION AND DISCUSSION OF RESULTS

The model was used to analyze the heating and cooling performance of the roof pond in four distinct climates: Phoenix, Arizona; Sacramento, California; Atlanta, Georgia; and Washington, D.C. In addition, sensitivity studies were performed to examine the influence on system performance of various engineering design parameters for both the heating and cooling modes of operation. For purposes of comparison, a standard set of system parameters is defined as a reference for both heating and cooling and is used throughout this study: these standard parameters are given in Appendix IV. The room temperature is assumed to be constant for each simulation.

The choice of the most effective strategy for insulation control, the results of the parametric studies, and the roof pond performance in various climates are discussed in the following sections.

III.1 STRATEGY FOR TOP AND BOTTOM INSULATION CONTROL

Different strategies were considered for controlling the opening and closing times of the top and bottom insulation. The relative merits of the individual strategies were judged in terms of their effectiveness in minimizing heat losses during the heating months or maximizing heat losses during the cooling season. The simplest logic considered was set times for opening and closing of top insulation and positioning the bottom insulation during a particular hour based on the relative temperatures of the steel deck and room air during the previous hour. More elaborate strategies were studied by simulating all four control possibilities (both insulations open; both closed; open top, closed bottom; closed top, open bottom) at the beginning of each hour. The most advantageous combination was then chosen by considering in turn parameters such as the heat flow rate between the steel decking and the room, the temperature of the pond water, or the temperature of the steel decking. None of these strategies seemed to be satisfactory. The strategy utilized in the simulations reported here is as follows: At the beginning of the hourly calculation, the roof pond is decoupled from the room by assuming the bottom insulation to be closed. The roof pond system is simulated with the top insulation in both closed and open positions; the position resulting in the higher (lower) net heat flow from outside into the system for the heating (cooling) mode is chosen. Given this position for the top insulation, the system performance is analyzed for each of the two possible positions for the bottom insulation; the position which results in higher heat flow into (out of) the room for the heating (cooling) mode is chosen. Table 2 shows the openning and closing times for the insulation panels in the four climates examined here assuming a 22^{o}C room air temperature.

III.2 PARAMETRIC STUDIES

All parametric studies reported here are based on the standard roof pond parameters given in Appendix IV; only the individual parameter being investigated is varied in a particular simulation. The room temperature is taken to be constant and equal to 22^{o}C for both the cooling and heating modes. The pond is always assumed to be covered by the evaporative layer during the cooling months and the strategy described in the previous section is adopted for manipulating the insulation layers in all simulations.

III.2.1 Top and Bottom Insulation Effect

For heating periods, the effect of the top insulation is to retain collected heat during sunless hours. The effect of the lower insulation is to supress undesirable losses under severely cold conditions. Figure 2 is a comparison of hourly values of heat flow rates into or out of the room for January in Phoenix for four different roof pond insulation designs; where one incorporates both insulations, two includes only top insulation, three uses only bottom insulation, and four has no insulation. The curves coincide for the systems with both top and bottom insulations and with only top insulation; this is due to the fact that for the Phoenix climate and the fixed room temperature, the bottom insulation is always open according to the control strategy described earlier. In fact, annual simulations demonstrated that the bottom insulation would never be closed in Phoenix if the cooling of the pond is evaporatively aided. However, the bottom insulation could be beneficial for other climates. For example, in Washington, D.C., the bottom insulation is always closed during the months of January, February, and December, and is utilized partially during the month of November. Similar usage of bottom insulation is observed in Sacramento and Atlanta.

The beneficial effects of top insulation on roof pond performance is clearly demonstrated in Fig. 2. The daily net heat gain for January in Phoenix is 2300 kJ-day^{-1}m^{-2} when both insulations are

TABLE 2. Insulation Control Strategy* (Room Temperature = 22°C)

LOCATION	JANUARY			AUGUST				
					With Evaporative Layer		Without Evaporative Layer	
	Sunrise/ Sunset	Top Insulation Open/Closed	Bottom Insulation Open/Closed	Sunrise/ Sunset	Top Insulation Open/Closed	Bottom Insulation Open/Closed	Top Insulation Open/Closed	Bottom Insulation Open/Closed
ATLANTA	8am/6pm	12 noon/4pm	Always Closed	6am/8pm	9pm/7am	Always Open	12 mid/7am	Always Open
PHOENIX	8am/6pm	10am/4pm	Always Open	6am/8pm	8pm/7am	Always Open	2am/7am	Always Closed
SACRAMENTO	8am/6pm	12 noon/4pm	Always Closed	6am/8pm	7pm/7am	Always Open		
WASHINGTON	8am/6pm	12 noon/4pm	Always Closed	6am/8pm	8pm/7am	Always Open		

*All hours are solar

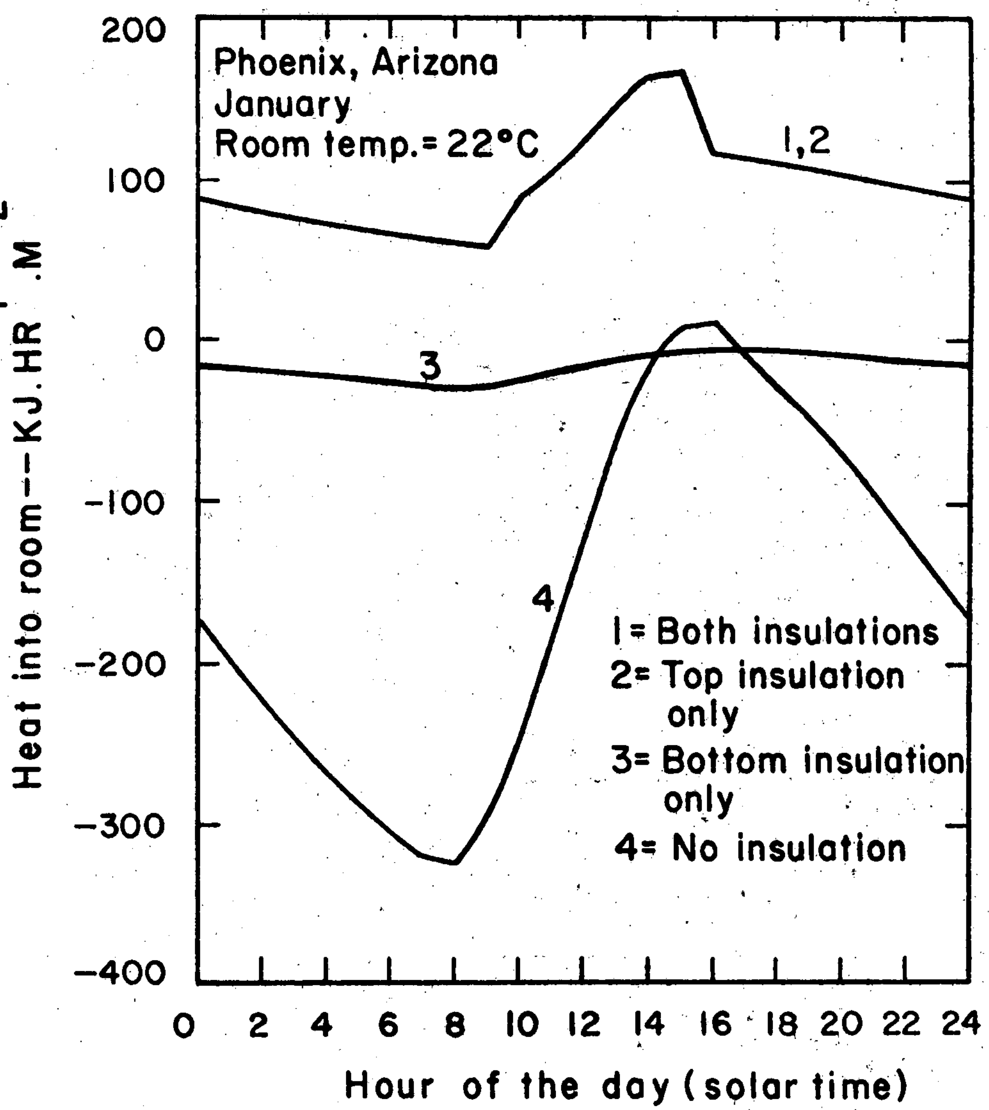

EFFECT OF TOP AND BOTTOM INSULATION ON HEATING PERFORMANCE OF THE ROOF POND

XBL 803-6660

utilized, compared to a heat loss of 3800 kJ-day^{-1}m^{-2} when no insulation is used. If only the bottom insulation is available, the heat loss would be reduced to 400 kJ-day^{-1}m^{-2}.

Figure 3 is a comparison of the same four roof pond insulation configurations for the month of August. The daily net heat loss for August in Phoenix is 1000 kJ-day^{-1} m^{-2} of roof area for both systems which include top insulation (the control strategy results in the bottom insulation remaining in the open position for the entire month). This should be compared with the case when neither insulation is used which results in a gain of 5100 kJ-day^{-1} m^{-2}.

Plots of hourly values of the temperature of the encased water for the four different system designs are presented in Fig. 4 for January in Phoenix. It is evident that the effect of top insulation is to increase the water temperature in the bag and reduce the daily temperature variation. Plots of dry bulb and wet bulb temperatures are also included in Fig. 4. Analogously, during a cooling month, use of the the top insulation results in a decrease of the temperature of the water in the bag.

III.2.2 Insulation Thickness

Annual simulations (12 days - 1 day per month) of roof pond performance were carried out for the Phoenix climate with top insulation thicknesses varying from 1 cm to 7 cm. For all of these studies, the control strategy resulted in the bottom insulation being open for the entire year. The results are shown in Figure 5, where the net daily heat gain or loss by the room is plotted as a function of insulation thickness for January and August. It can be seen that increasing the thickness of the top insulation improved the performance of roof pond during both the heating and cooling periods. In this climate, the performance improvement becomes less significant for thicknesses above 3 cm. The effect of top insulation thickness on hourly heat gains or losses by the room is demonstrated in Figs. 6 and 7.

III.2.3 Water Pond Depth

The effect of water pond depth on roof pond performance was investigated by simulating ponds with depths ranging from 5 to 30 cm. Figure 8 shows the daily heat gains or losses of the room as a function of water depth for two months during the heating season--January and February--and a month during the cooling season--August. The net gain in the heating mode increases as the pond depth is increased from 5 to 15 cm; further increases of pond depth have no

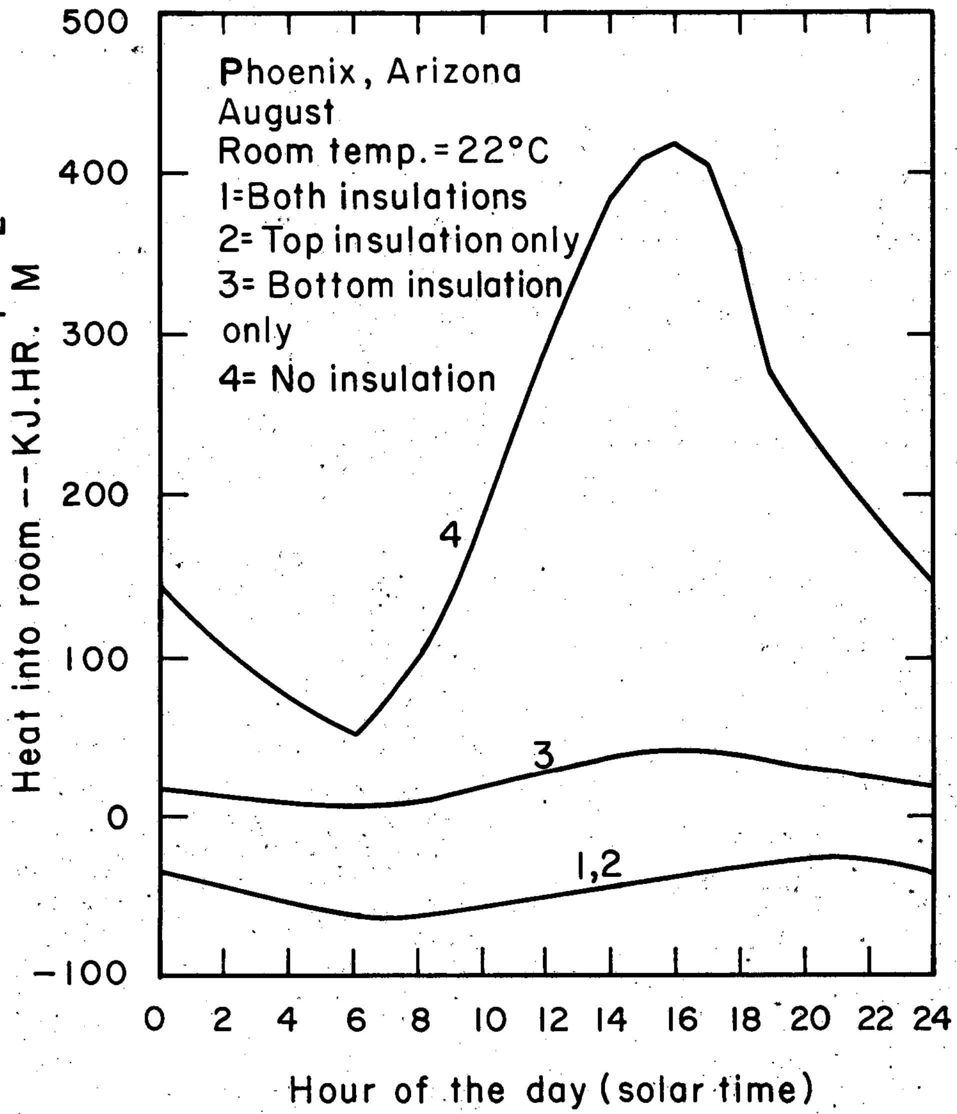

EFFECT OF TOP AND BOTTOM INSULATION ON COOLING PERFORMANCE OF THE ROOF POND (EVAPORATIVELY AIDED)

XBL803-6661

FIGURE 3.

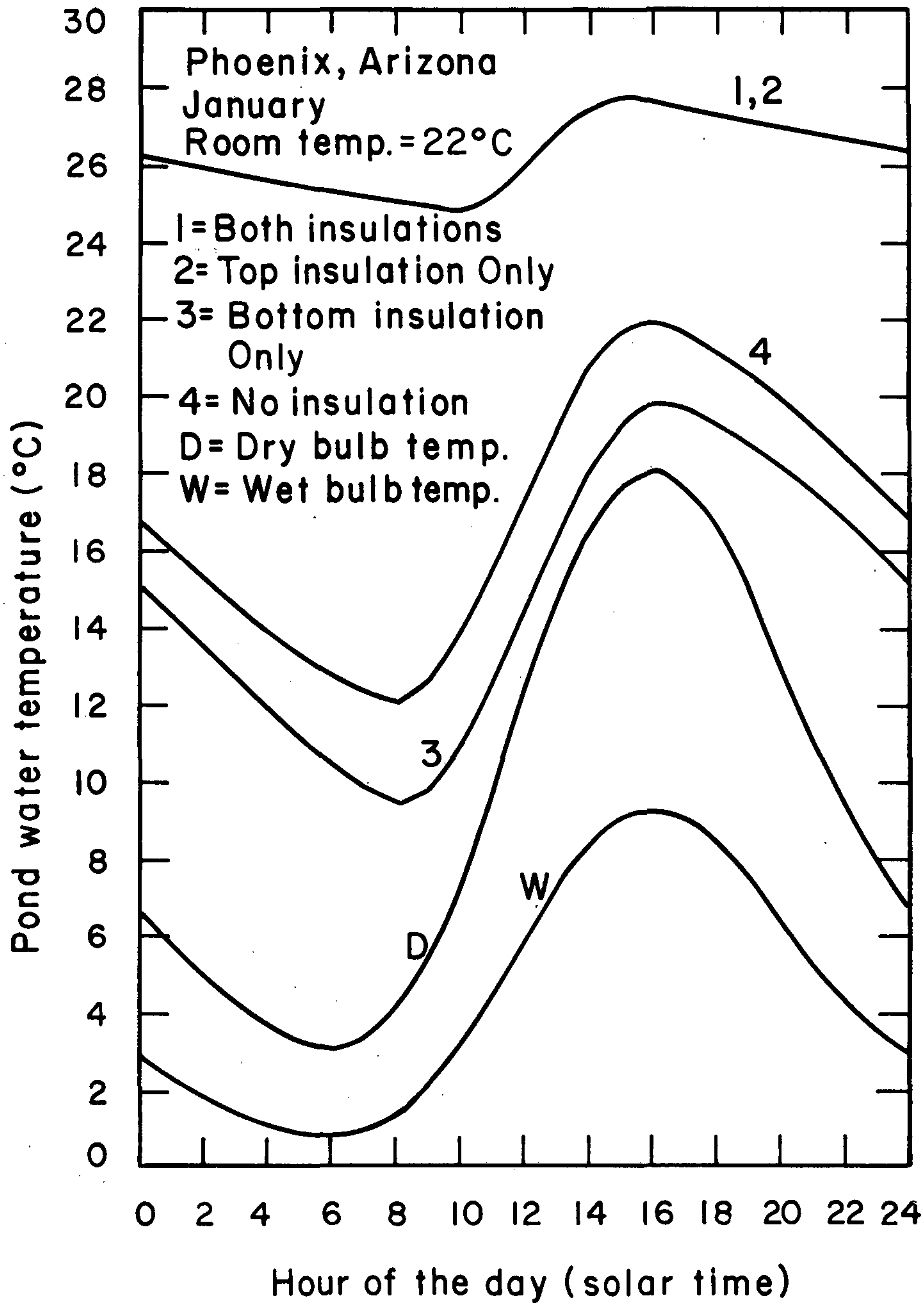

EFFECT OF TOP AND BOTTOM INSULATION ON
POND WATER TEMPERATURE IN WINTER

XBL 803-6662

FIGURE 4.

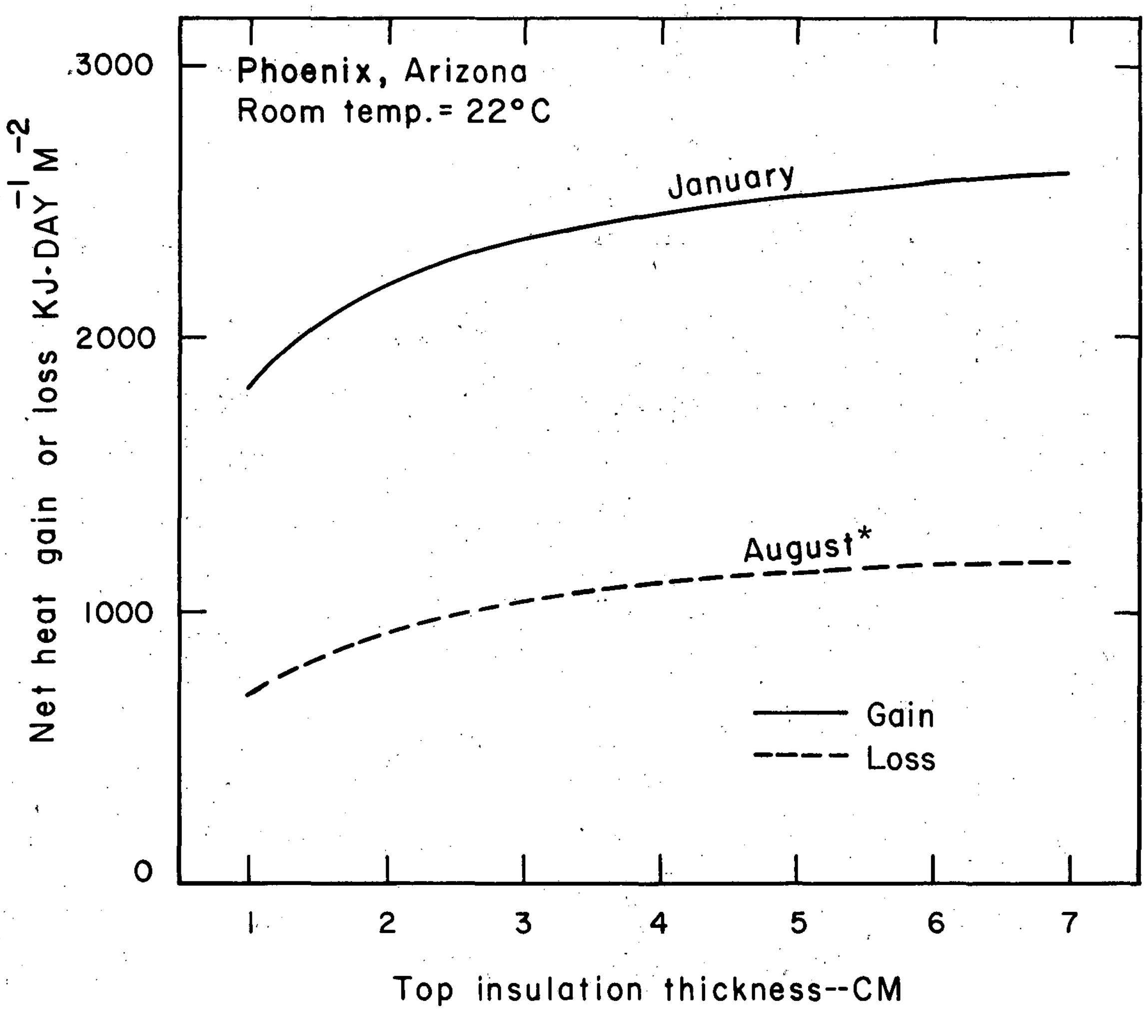

EFFECT OF TOP INSULATION THICKNESS
ON THE DAILY HEAT GAIN OR LOSS

XBL 803-6663

*Evaporatively Aided

FIGURE 5.

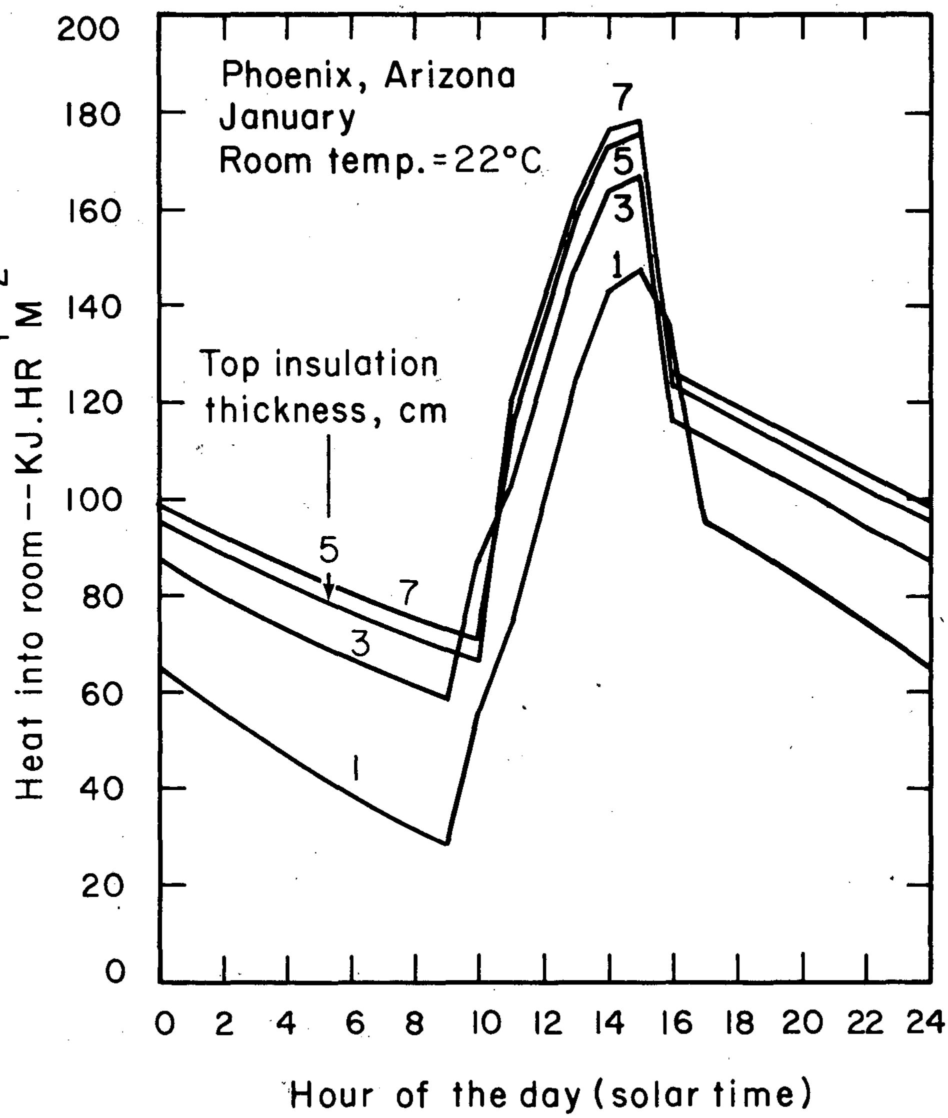

EFFECT OF TOP INSULATION THICKNESS ON
HEATING PERFORMANCE OF THE ROOF POND

XBL803-6664

FIGURE 6.

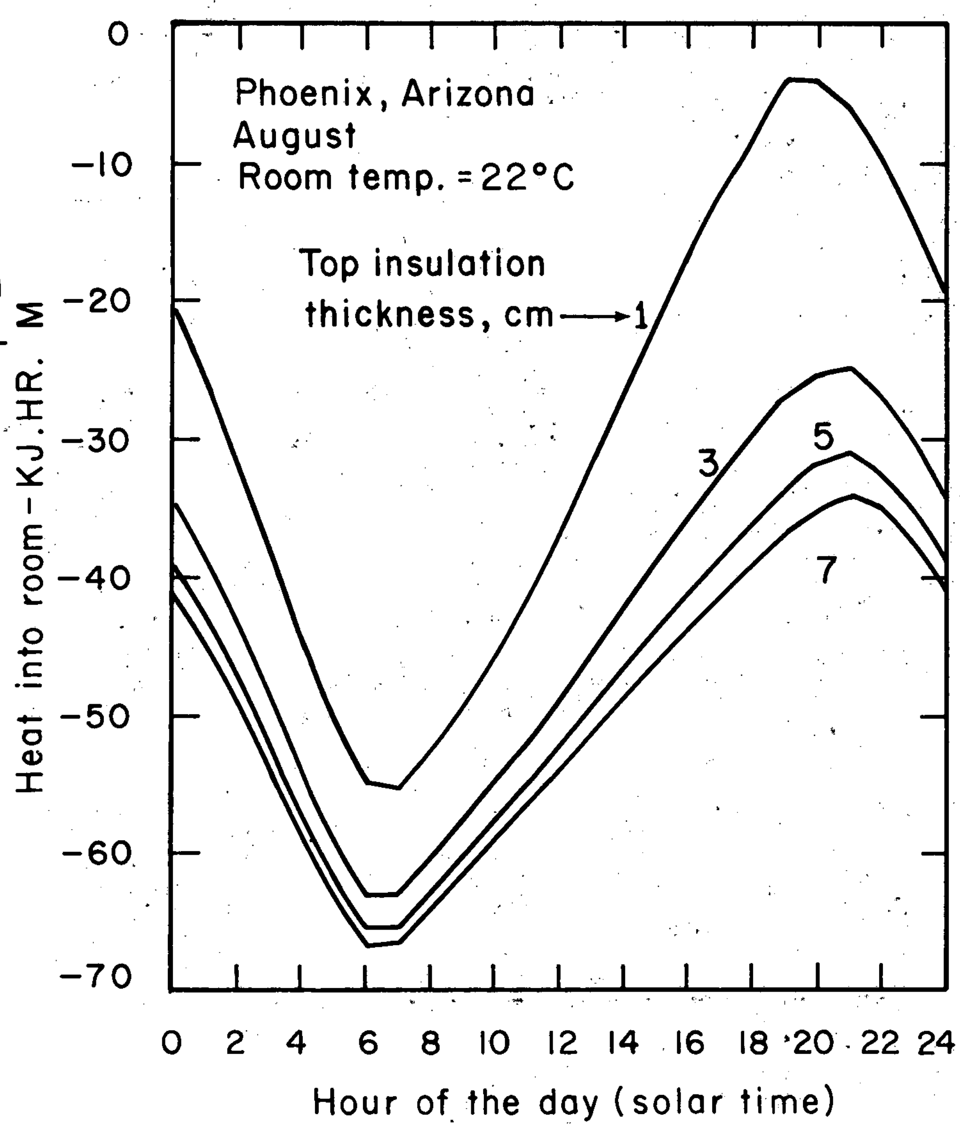

EFFECT OF TOP INSULATION THICKNESS ON COOLING PERFORMANCE OF THE ROOF POND (EVAPORATIVELY AIDED)

XBL 803-6665

FIGURE 7.

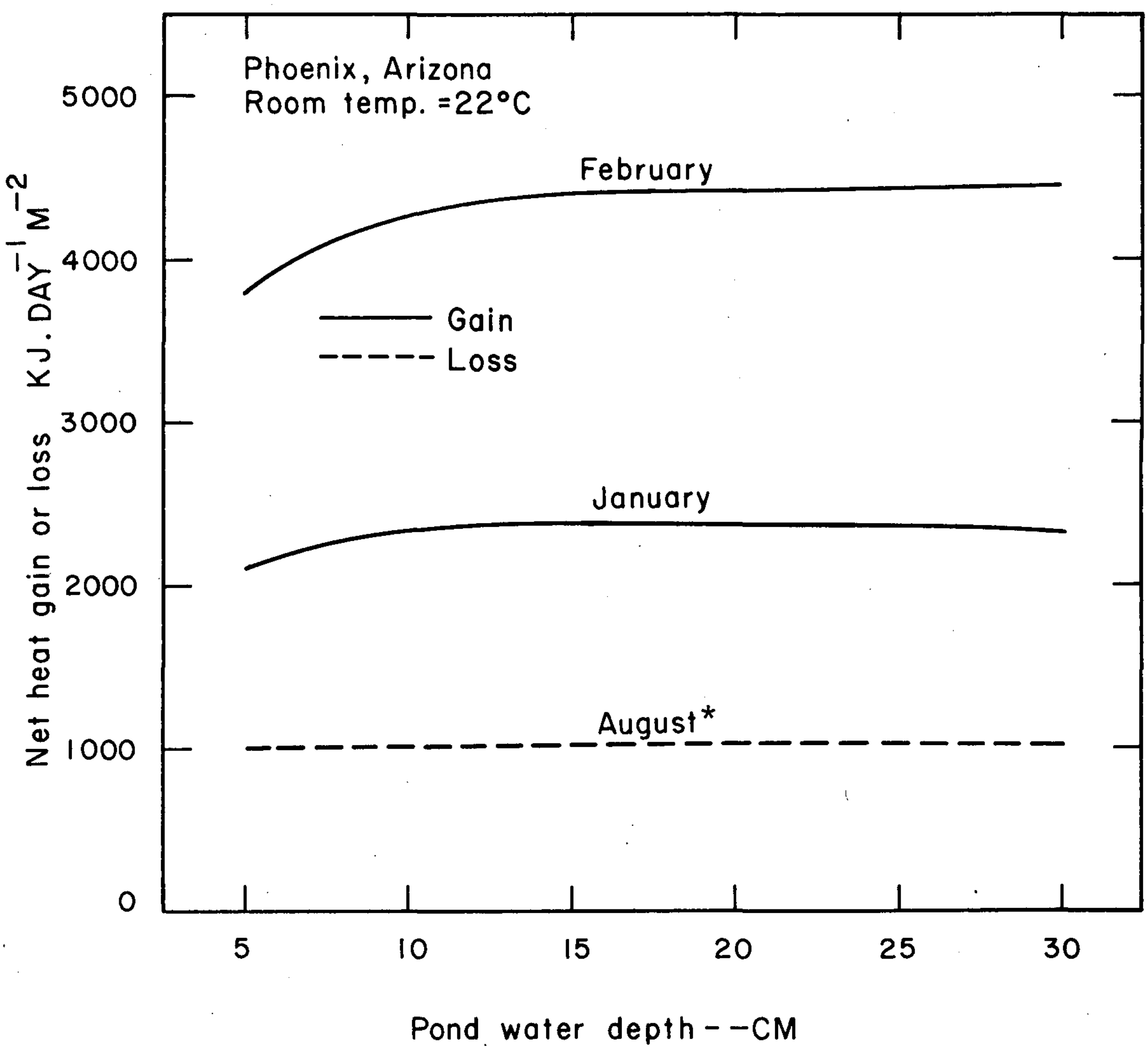

EFFECT OF POND WATER DEPTH ON
THE DAILY HEAT GAIN OR LOSS

XBL 803-6666

*Evaporatively Aided

FIGURE 8

significant effect on heat gain. During the cooling months, increasing the pond depth from 5 to 15 cm improves the roof pond performance only slightly; the performance benefits of increased water depth are significantly less than those realized during the heating season.

The net daily gain or loss of heat by the room is one measure of the effectiveness of the passive solar system. However, significant daily variations of heat flow in or out of the room may be accompanied by uncomfortable variations in room temperatures. Figures 9 and 10 show the heat flow in or out of the room as a function of time of day for different pond depths. As the pond thickness is increased the daily range of variation of heat flux into the room is decreased. Therefore, although Fig. 8 suggests that the total daily cooling effect in Phoenix remains almost unchanged with pond depth variations, Fig. 10 clearly shows that a deeper pond may provide more stable comfort conditions. Any conclusions concerning the comfort conditions should, however, include the thermal mass of the entire buiding. The daily variation of pond water temperature for various pond depths is presented in Figs. 11 and 12.

III.2.4 Evaporative Layer Effect

The cooling potentials of a roof pond both with and without an evaporative layer have been examined for August in Phoenix, Arizona, and Atlanta, Georgia. The results show that in Phoenix, 1000 kJ-day^{-1} m^{-2} of heat can be removed from the room when an evaporative layer is used, whereas without an evaporative layer the room actually gains 100 kJ-day^{-1} m^{-2}. For Atlanta, 800 kJ-day^{-1} m^{-2} of heat is removed by using evaporative enhancement, as compared with 400 kJ-day^{-1} m^{-2} without the evaporative layer. The hourly values of heat flux from the roof pond into the room, both with and without an evaporative layer, are presented in Figs. 13 and 14. Values of evaporative, radiative, and convective-conductive heat fluxes from the roof to the environment are shown in these figures for those hours that the top insulation is open.

Examination of Figs. 13 and 14 reveals that the evaporative heat losses are the sole reason for improving the roof pond performance in both Phoenix and Atlanta. The radiative heat losses to the sky are, in fact, larger in Phoenix when the roof pond is not covered by an evaporative layer. The combined convection-conduction heat transfer from the ambient air to the dry plastic surface is expected to be smaller than that to the evaporative layer surface because of the relative values of these surface temperatures in the two cases. Such behavior is not consistently observed in Figs. 13 and 14; this is explained by the fact that two different equations (Eq. (17) and (19) in section II.1.1.3) are used to estimate the convective-conductive heat transfer coefficient between ambient air

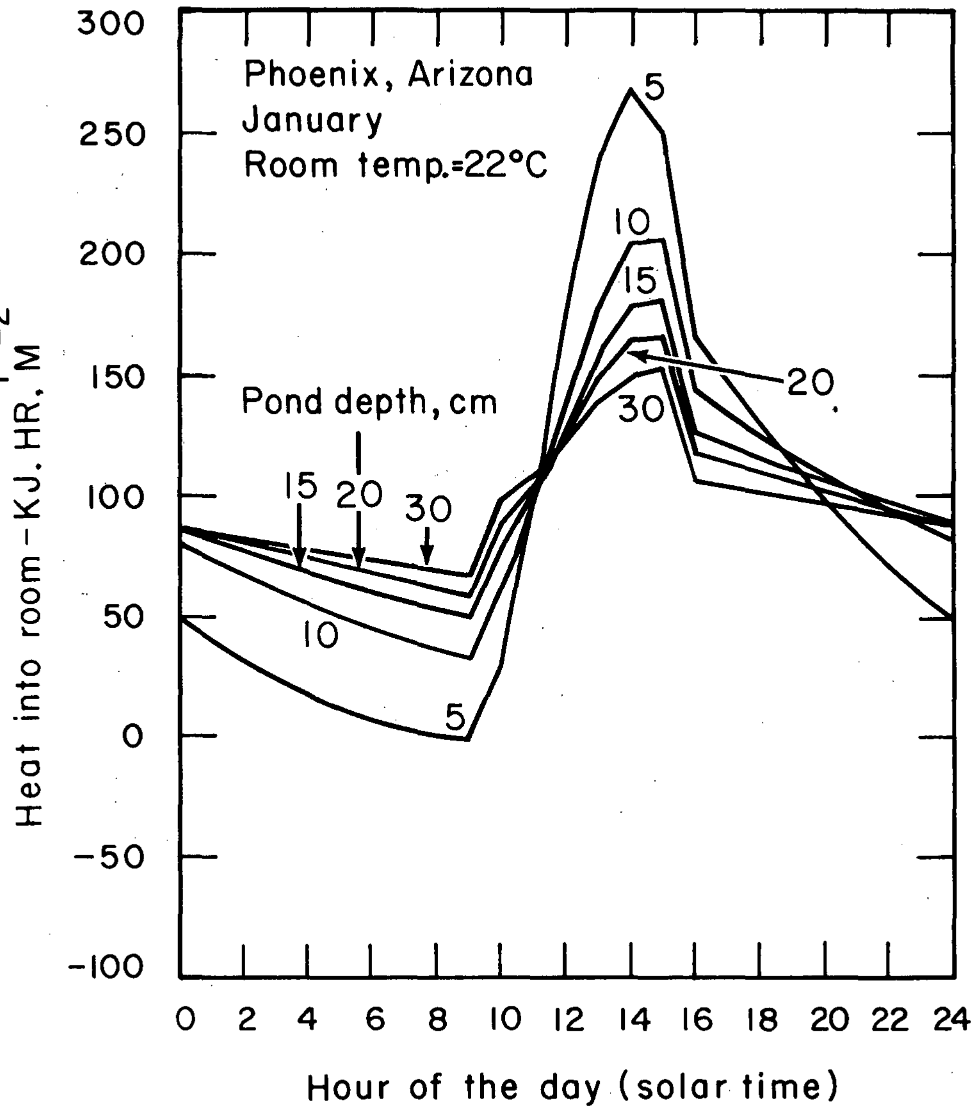

EFFECT OF POND DEPTH ON HEATING
PERFORMANCE OF THE ROOF POND

XBL803-6667

FIGURE 9.

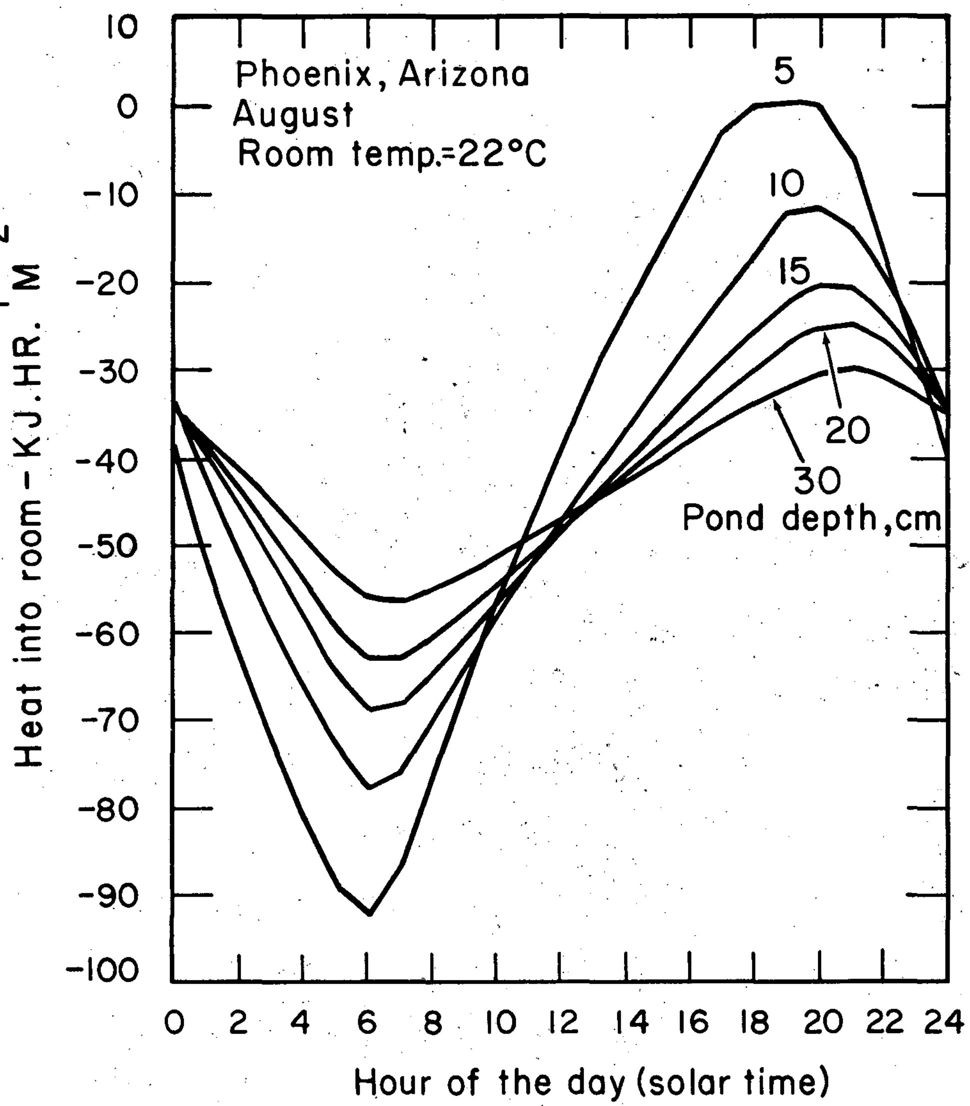

EFFECT OF POND DEPTH ON COOLING PERFORMANCE OF THE ROOF POND (EVAPORATIVELY AIDED)

XBL803-6668

FIGURE 10.

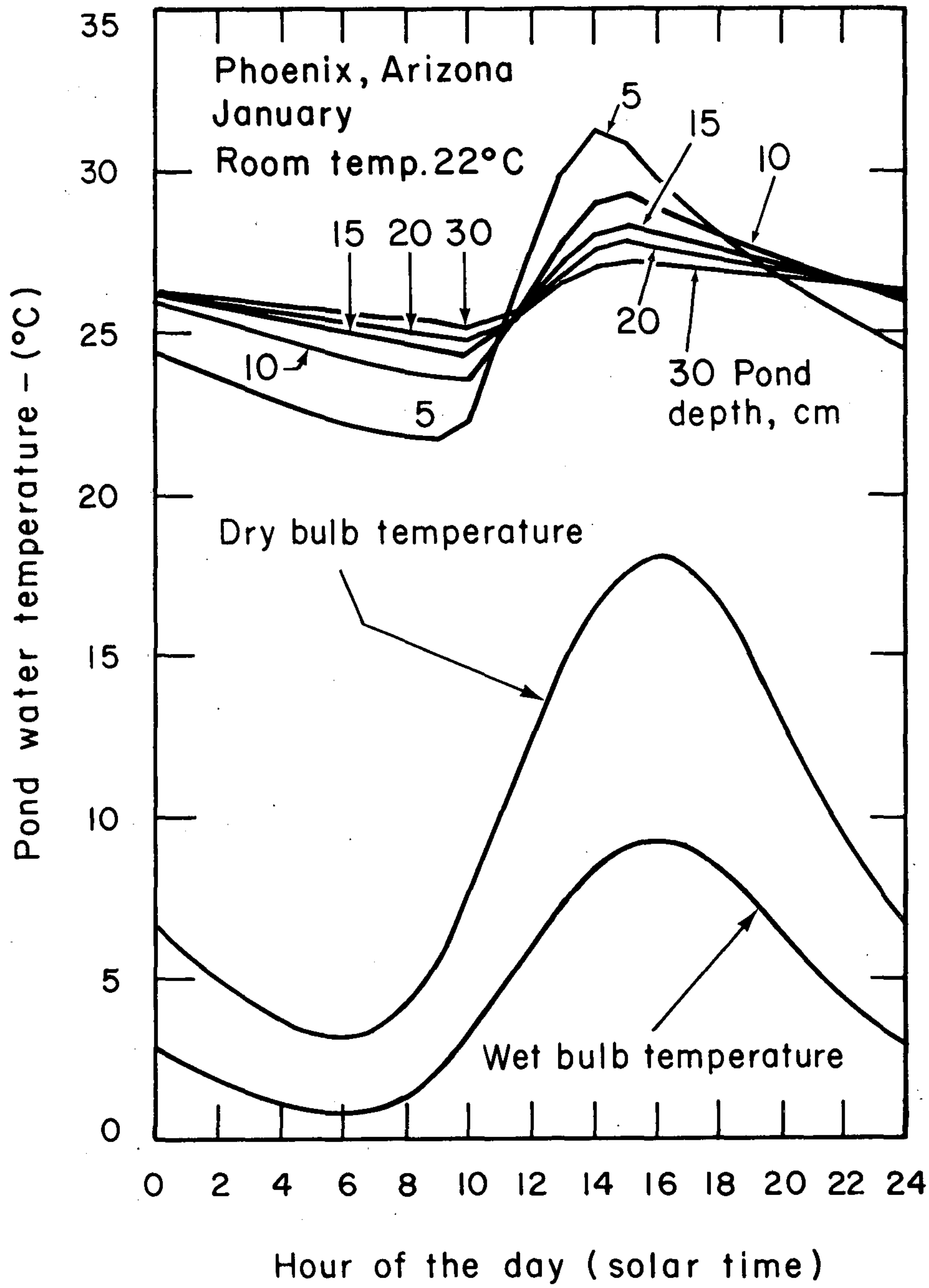

EFFECT OF POND DEPTH ON POND
WATER TEMPERATURE IN WINTER

XBL 803-6669

FIGURE 11.

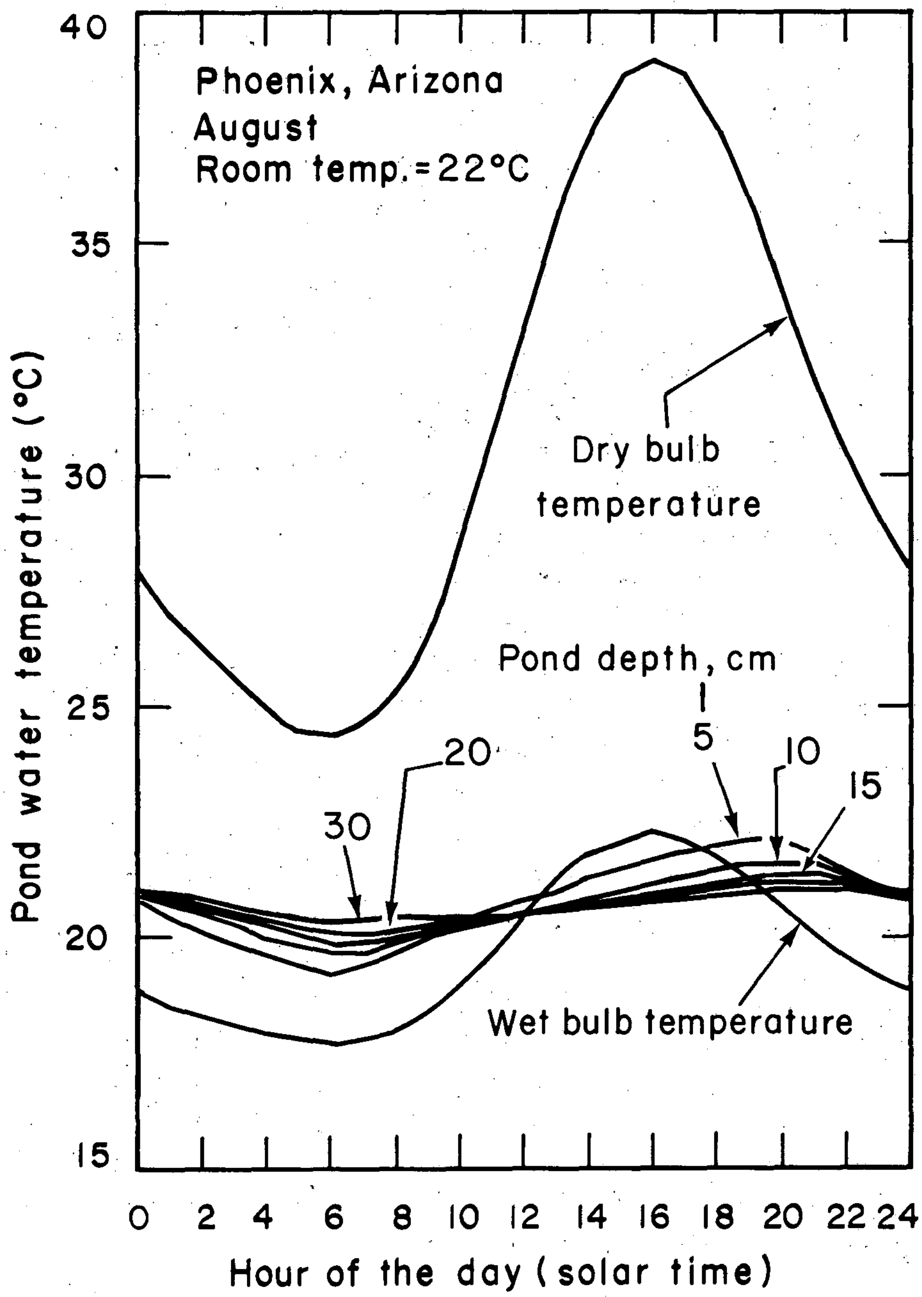

EFFECT OF POND DEPTH ON POND WATER TEMPERATURE IN SUMMER (EVAPORATIVELY AIDED) XBL803-6670

FIGURE 12.

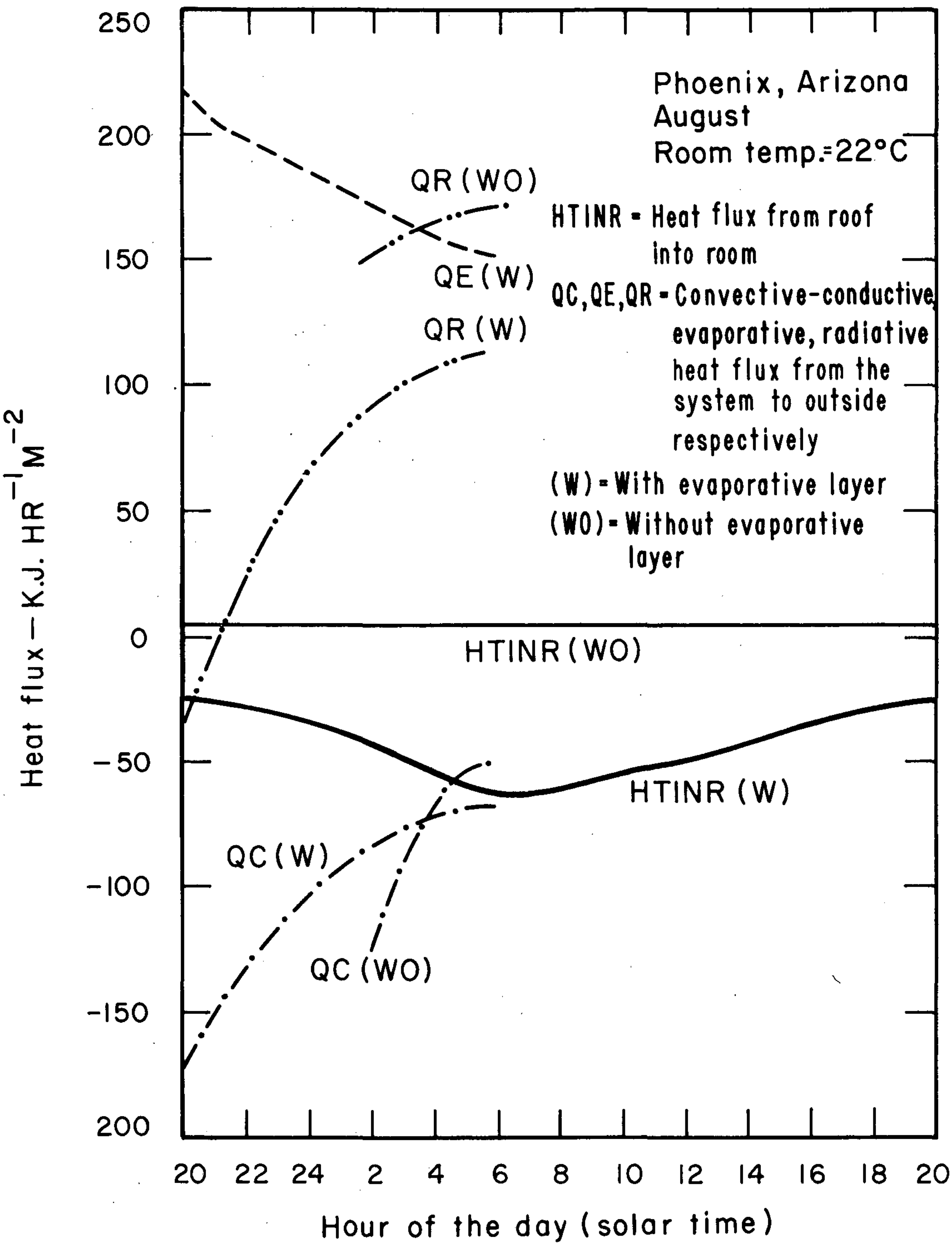

EFFECT OF EVAPORATIVE LAYER ON COOLING PERFORMANCE OF THE ROOF POND

XBL 803-6679

FIGURE 13.

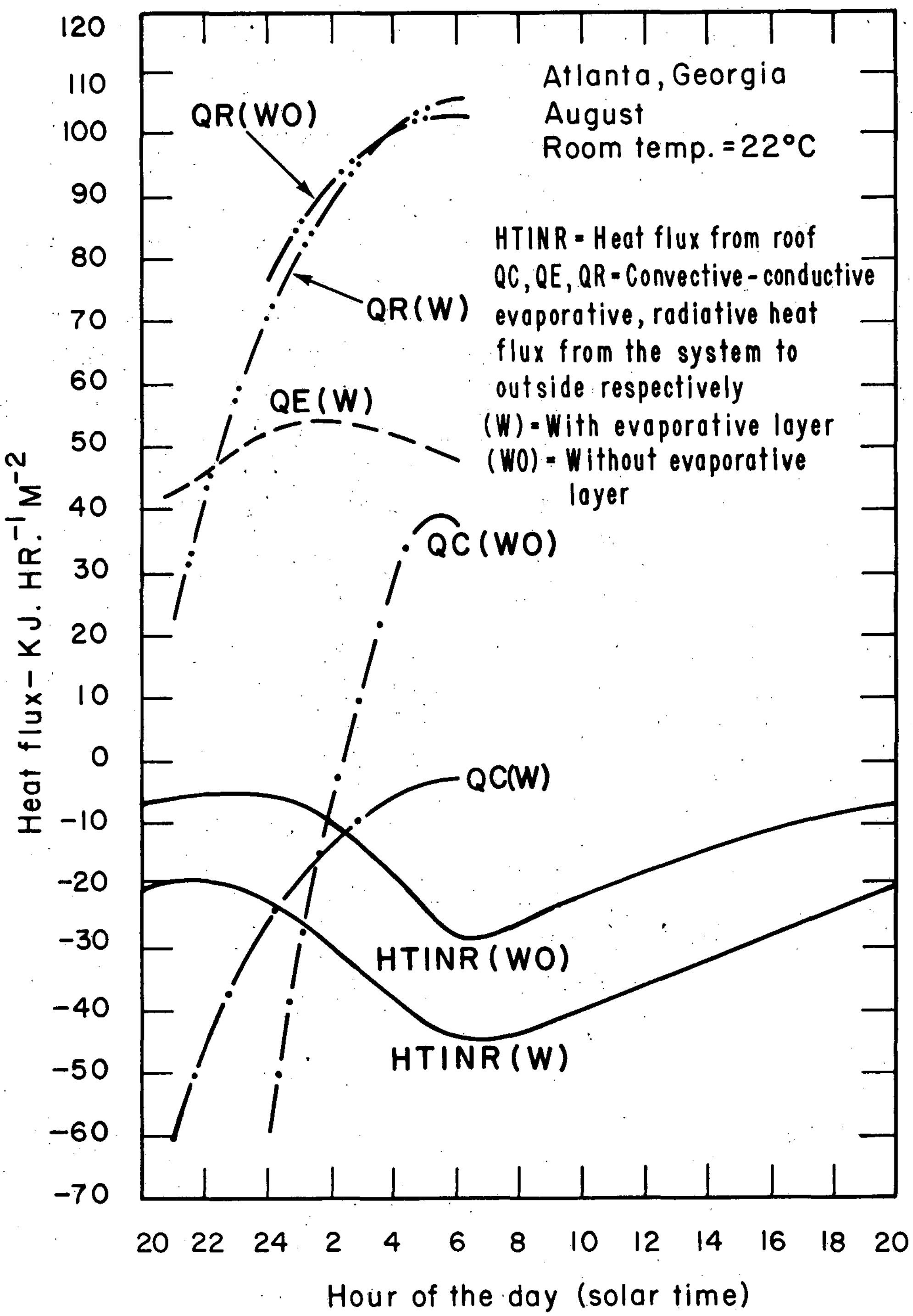

EFFECT OF EVAPORATIVE LAYER ON COOLING PERFORMANCE OF THE ROOF POND

XBL 803-6680

FIGURE 14.

and (1) the dry plastic surface, or (2) the evaporative layer surface. The validity of Eq. (17) is particularly questionable.

III.2.5 Evaporative Layer Thickness

The results of varying the evaporative layer thickness are shown in Fig. 15. It appears that the depth of the evaporative layer does not have a significant effect on the cooling potential of the roof pond.

III.3 ROOF POND HEATING AND COOLING POTENTIALS

The heating and cooling performance of roof pond systems is studied in four different climates, Atlanta, Georgia; Phoenix, Arizona; Sacramento, California; and Washington, D.C. The simulations use the standard parameters and dimensions described in Appendix IV. The energy saving potentials of the system are studied for constant interior temperatures ranging from 16 to 28^{o}C. The monthly results are summarized in Figs. 16-19, where the net daily heat gains by the occupied space per unit area of the roof are shown as functions of room temperature. Since the building loads are not being calculated in the simulations, the decisions as to whether the roof pond should be in the heating mode or a cooling mode for a particular day is based on the heating or cooling degree days calculated with 18.3^{o}C as a basis. It is readily seen that a significant advantage may be realized if slight accommodations are permitted in the room thermostat setting.

A thorough assessment of roof pond potentials for heating and/or cooling is only possible when the model is incorporated into a building energy analysis program such as BLAST. The performance of such a passive solar structure can then be contrasted against that of a conventional building. However, in order to establish an energy consumption scale to which the roof pond performance can be compared, the heating and cooling loads for a typical building (excluding the roof) and the roof pond performance are shown in Figs. 20 and 21 for January and July respectively. The conventional building loads are calculated using an effective U-value based on the floor area and the difference between the room temperature and a mean monthly ambient temperature. The U-value was taken to be 200 kJ-m^{-2} ^{o}C^{-1} day^{-1}, which is typical for a single family detached house with a floor area of 120m^{2} This value agrees very well with that estimated, for the Atascadero experimental residence, by Niles [6]. The load for the building in its entirety (including the roof) may be estimated by adding approximately 25 percent to the values found in Figures 20, 21.

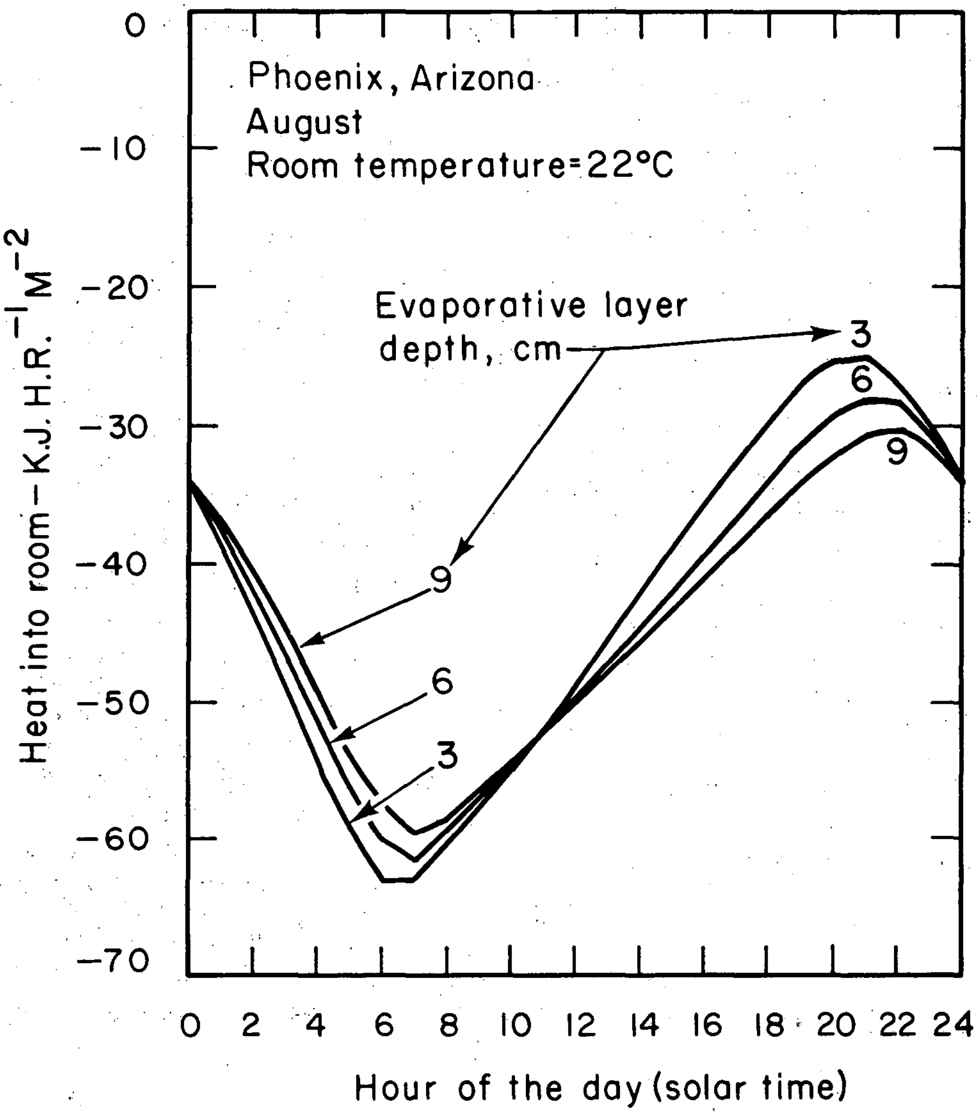

EFFECT OF EVAPORATIVE LAYER DEPTH ON
COOLING PERFORMANCE OF THE ROOF POND

XBL803-6681

FIGURE 15.

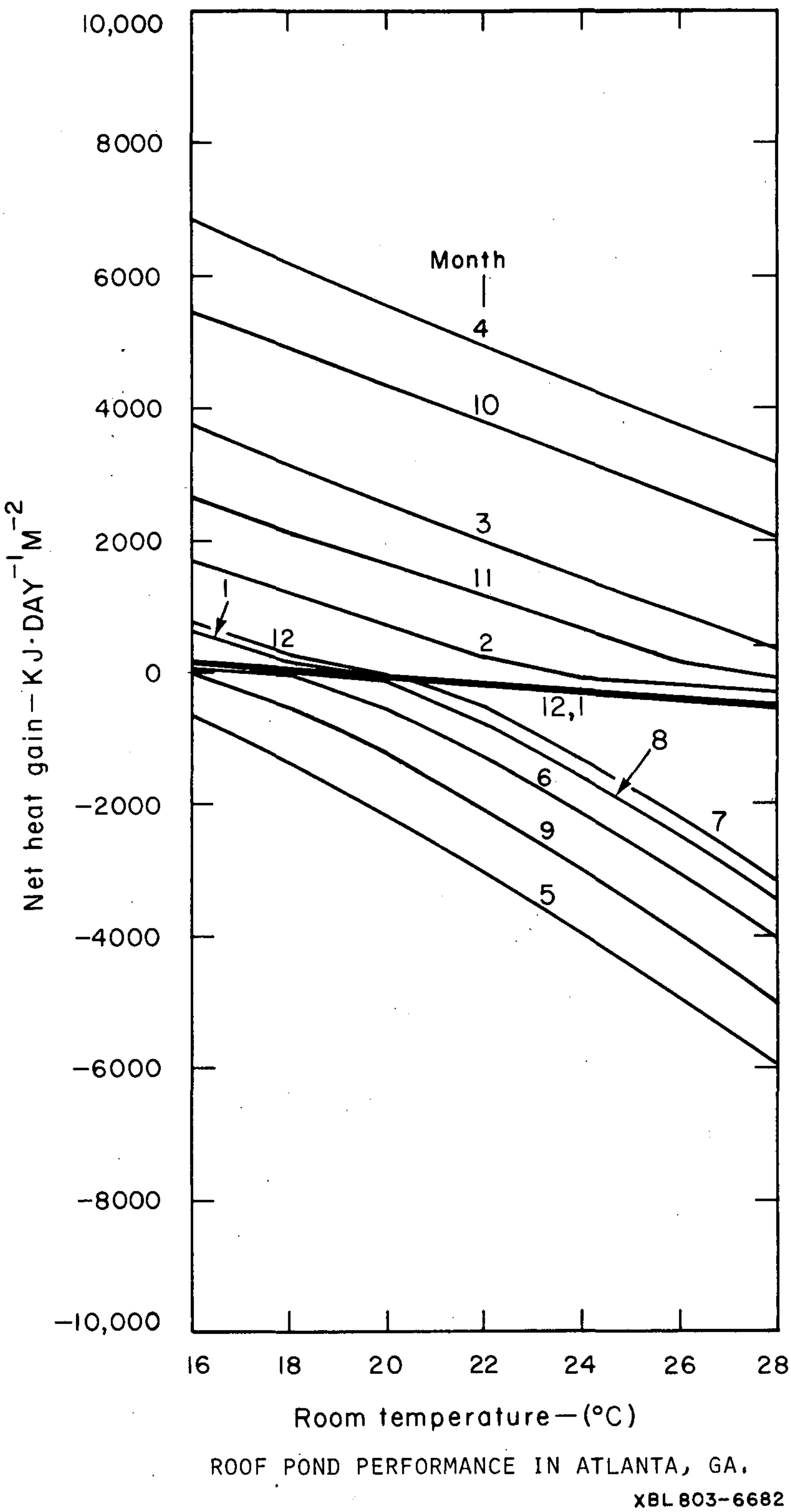

FIGURE 16. The pond is assisted evaporatively for months 5-9

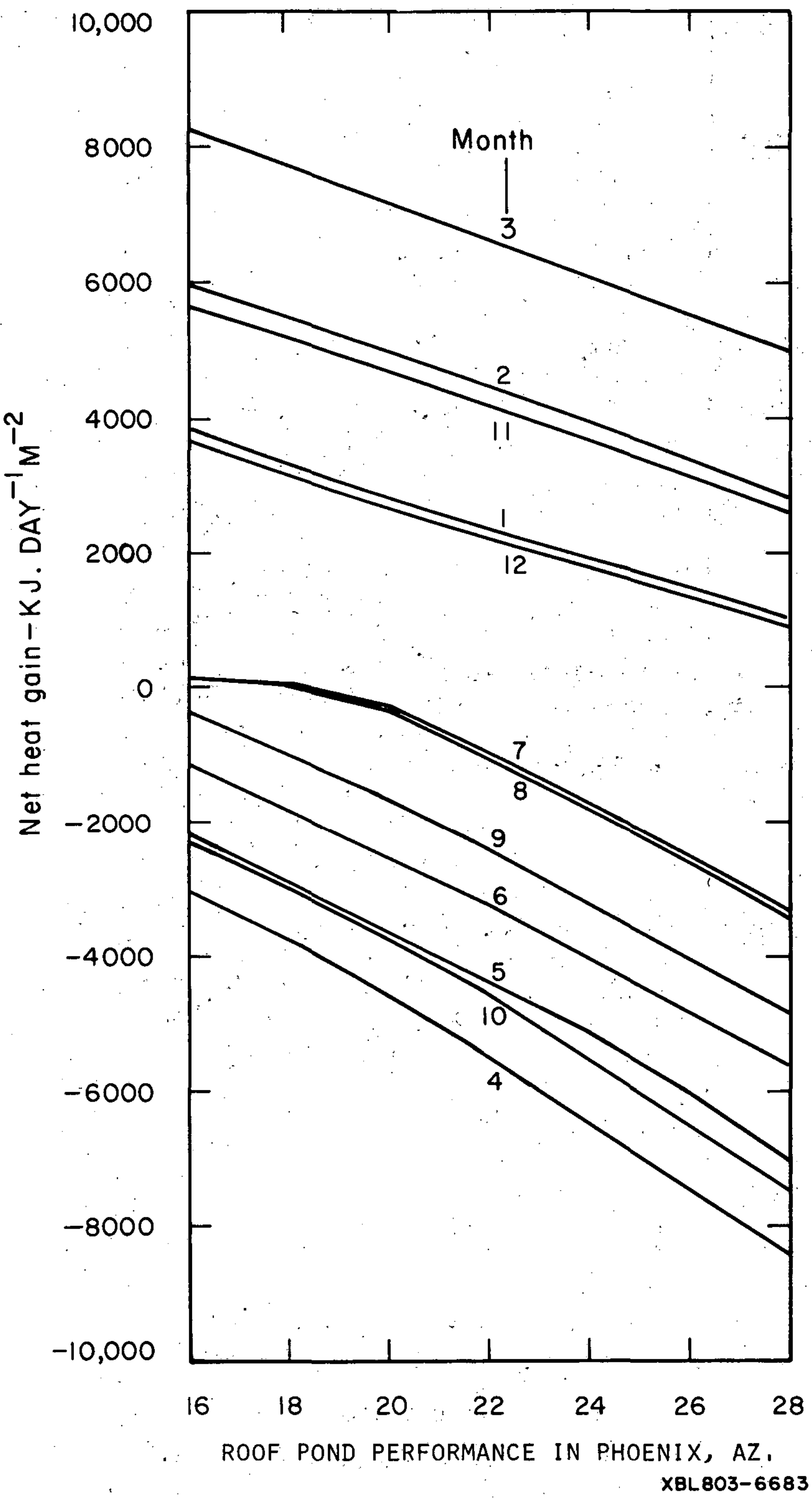

FIGURE 17. The pond is assisted evaporatively for months 4-10

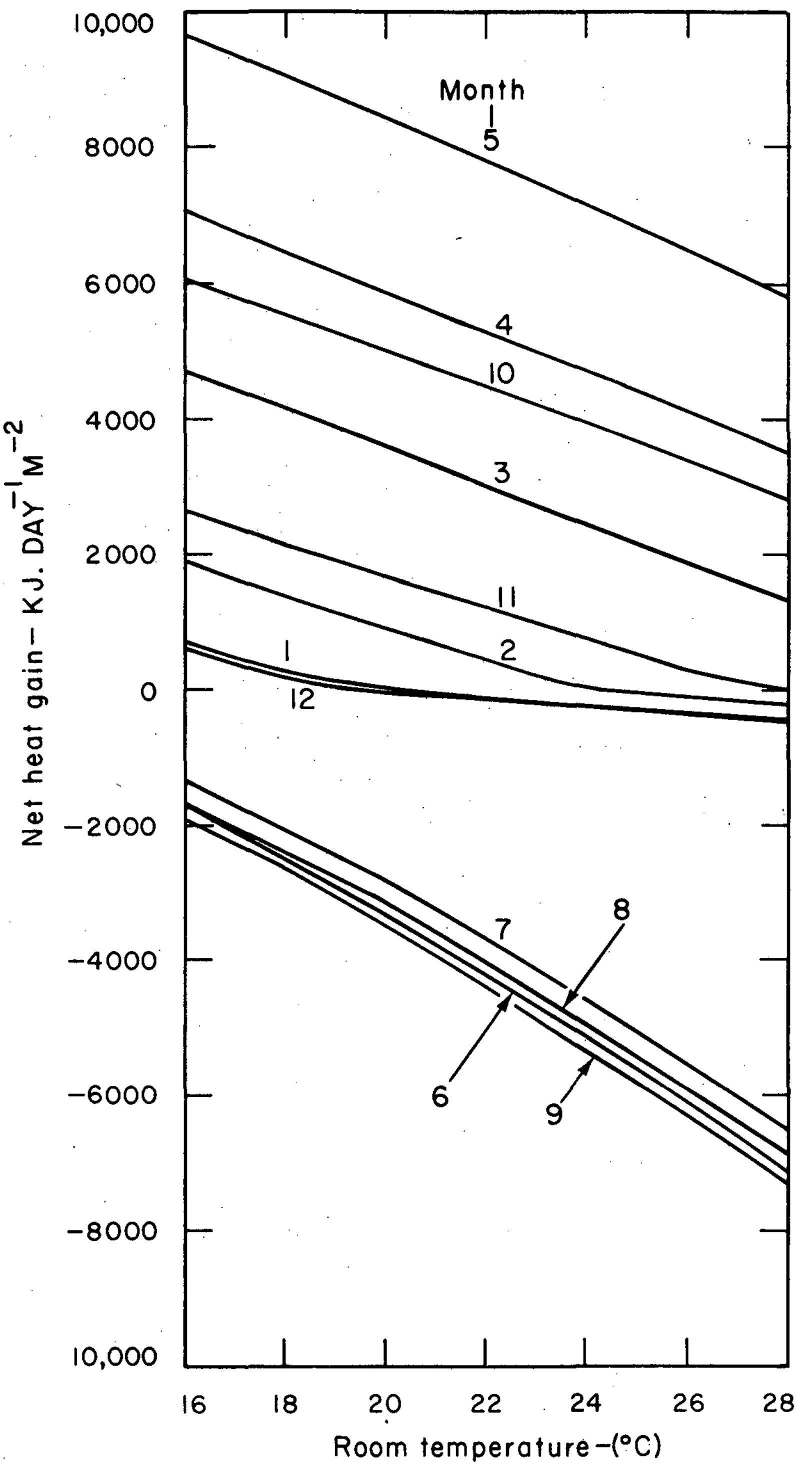

ROOF POND PERFORMANCE IN SACRAMENTO, CA.

XBL803-6684

FIGURE 18. The pond is assisted evaporatively for months 6-9

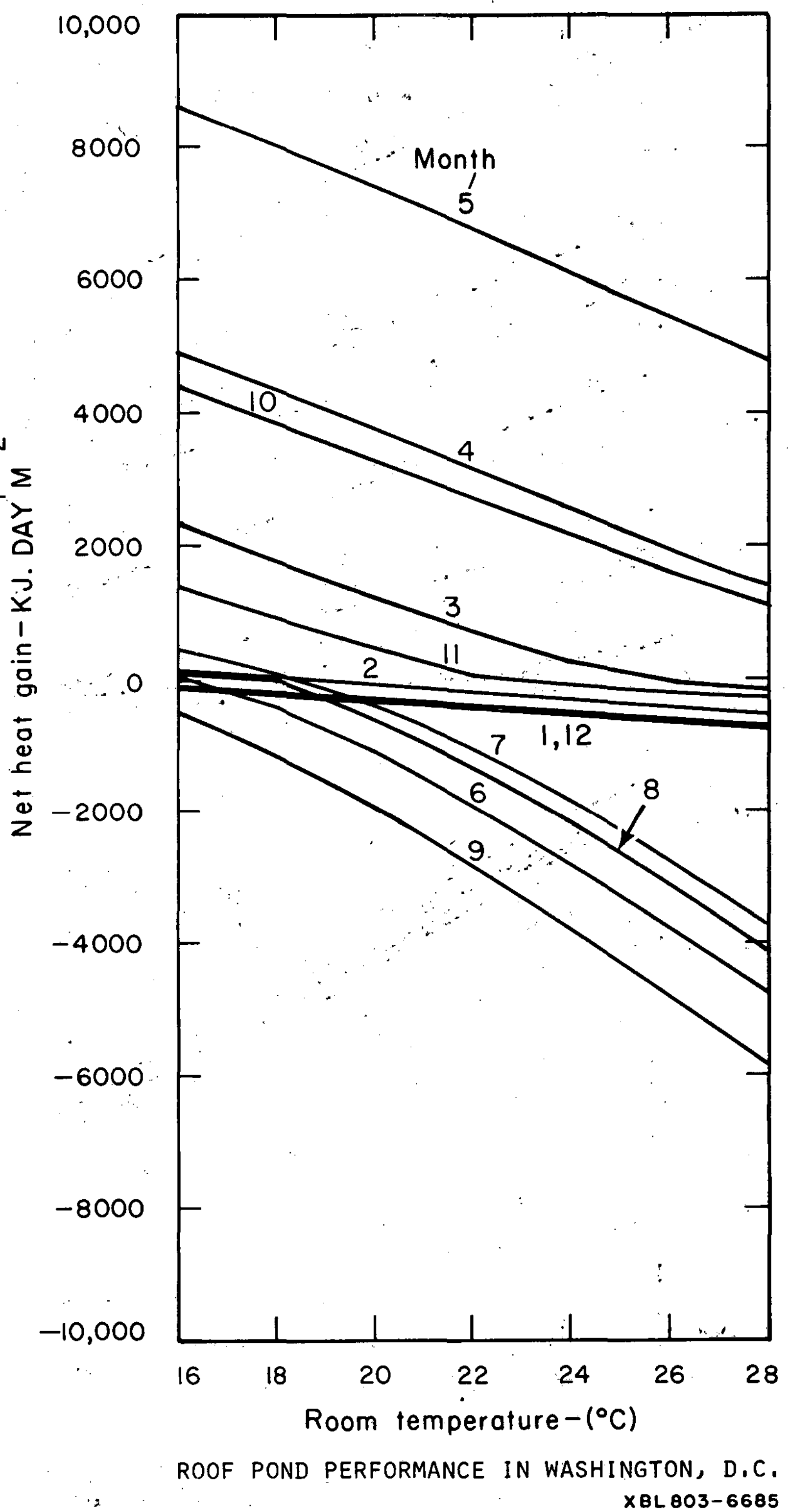

FIGURE 19. The pond is assisted evaporatively for months 6-9

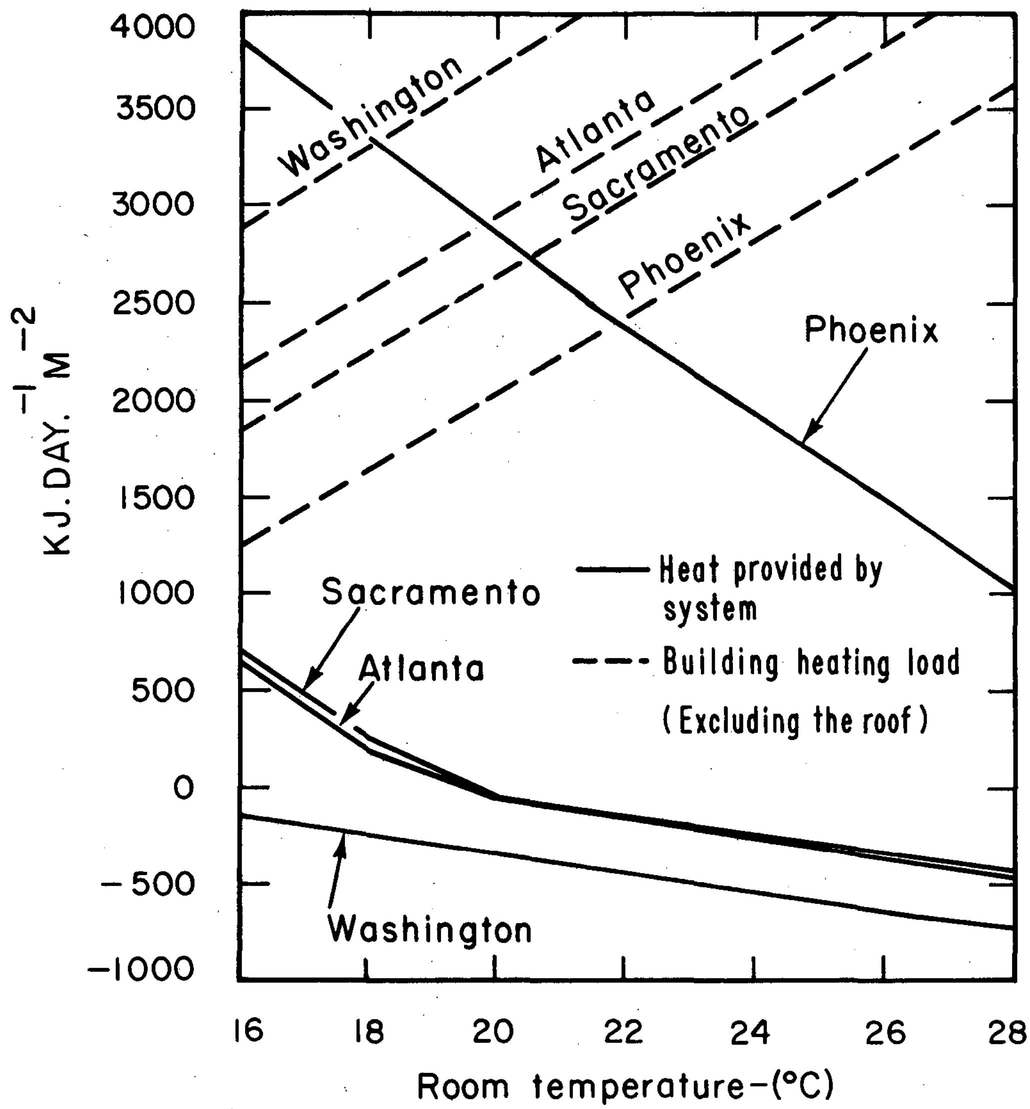

HEAT PROVIDED BY THE ROOF POND AND TYPICAL BUILDING HEATING LOADS FOR JANUARY

XBL 803-6686

FIGURE 20.

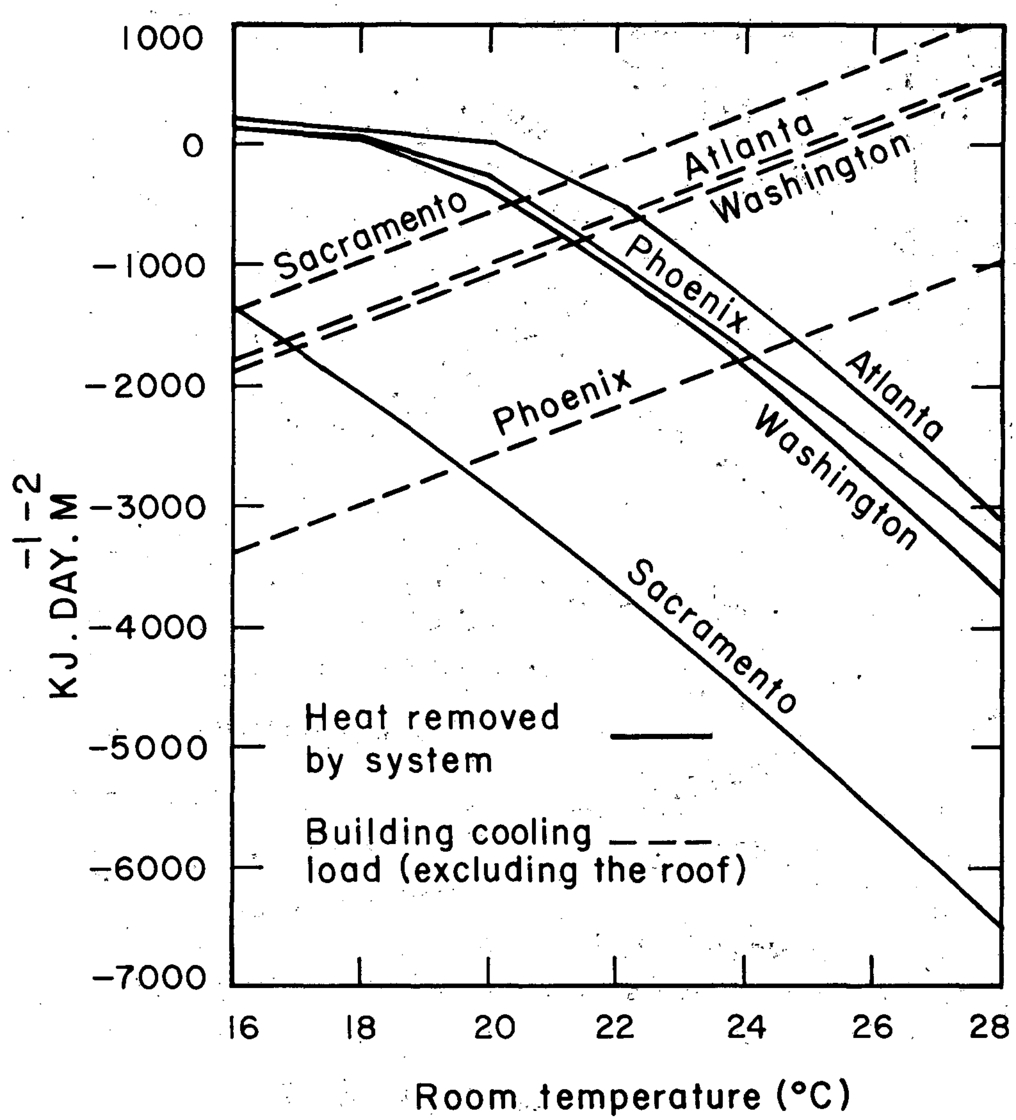

HEAT REMOVED BY THE ROOF POND AND TYPICAL BUILDING COOLING LOADS FOR JULY

XBL803-6687

FIGURE 21.

Present construction codes may reduce the building heating/cooling loads shown in Figs. 20 and 21 by up to a factor of 4. This load reduction enhances the attractiveness of roof ponds as an important passive architectural option. Figure 20 suggests that the heating needs of a typical residential building in Phoenix can be easily met by a roof pond with the specifications used in the model described here. For the cities of Atlanta, Sacramento, and Washington the heating season performance of the roof pond designs examined here does not appear especially attractive. It should be stressed that the heating performance of the roof pond can be improved by including inflatable air cells over the water bags. Examination of Figure 21 shows that the cooling potentials of the roof pond in the cities of Atlanta, Sacramento, and Washington appear to be comparable to the cooling loads in these climates. In Phoenix it appears that essentially all of the cooling needs could be met by allowing the room temperature to rise to approximately 24^{o}C.

IV. CONCLUSIONS

A flexible model of a roof pond system using empirical relations to determine the heat transfer coefficients for each of the different surfaces has been developed. The model utilizes an insulation panel control strategy which provides near optimal performance. The model will be incorporated in BLAST to permit rapid trade-off analysis of roof ponds in comparison to other passive and conventional building systems.

The model has been used to investigate the system performance sensitivity to the major roof pond design parameters. The major results of these studies are:

- The dynamic behavior of the roof pond is sensitive to the level of the top insulation. In Phoenix, however, there is little benefit to polyurethane insulation thicknesses over 3 cm. This suggests that for further improvement of the system performance, efforts may have to be concentrated on reducing infiltration losses from the panels rather than increasing the insulation level.

- Considering only its effect on total heat gain/loss from the occupied space--and neglecting its effect on occupant comfort level--the use of movable insulation between the roof pond and the occupied space would be of questionable thermal merit.

- While the overall daily performance of the roof pond is relatively insensitive to the pond depth, the hourly results vary substantially; this suggests that use of models which predict daily average performance may be misleading.

- An evaporative layer improves the cooling performance of the roof pond, but its thickness has negligible effect.

The model has also been used to investigate the heating/cooling potentials of the roof pond for four climates. Space cooling is the most important role in the four cities studied; only in Phoenix is the heating load of a typical residence met by the roof pond design used in the model described here. The relatively poor heating season performance of the system in the other three cities is not surprising; the addition to the model of an upper glazing would be desirable. Significant improvement in performance is possible if some flexibility of conditioned space temperatures is permitted. The comparisons of the roof pond performance with typical building heating/cooling loads presented above should only be considered as an indication of its application. A more reliable assessment of the system may be obtained once the model is incorporated in a complete building energy analysis code.

V. FUTURE WORK

The model described in this report uses many empirical relations and several simplifying assumptions. In order to better understand the limitations of the model more clearly, to improve the accuracy and reliability of its predictions and to increase its flexibility it is necessary to do further sensitivity studies, improve some of the simplifying assumptions and add more options to the model. The following tasks are considered to be important in future work:

(1) Perform sensitivity studies on many parameters involved in the simulation procedure. The results of these studies will define the most significant heat transfer mechanisms in the model and thereby indicate areas that might need further investigation.

(2) At present the model neglects infiltration between the outer insulation panel and the water pond; this is highly construction dependent. To first order, infiltration will have the same effect on roof pond performance as a decrease in top insulation level. To the authors knowledge, infiltration rates have not been measured in systems of this type; in practice, they may be the limiting factor in the net level of the top insulation. The model must be modified to consider this effect.

(3) The convective-conductive heat transfer coefficient between the outer insulation (or plastic surface) and the ambient air is estimated by Eq. (17). The validity of this equation for typical roof dimensions is open to question, and must be

examined.

(4) The model assumes the steel decking to be the only support for the water bags. In practice, however, the deck structure on which the water bags rest often includes a layer of concrete. Such an option should be included in the model.

(5) To increase solar energy collection efficiency, inflatable air-cells can be included over the water bags. It would be desirable to include a heat balance treatment for such an optional membrane in the model.

(6) The model does not at present differentiate between direct and diffuse radiation. The model should be modified to consider these two separately.

(7) Last, but not least, the model validity must be verified by comparing some experimental measurements with those predicted by the model.

Until the simulation model is developed to include some additional construction details of the roof pond, no serious validation studies can be initiated. However, a preliminary comparison of predictions and experiments of the Atascadero residence appears to be qualitatively satisfactory; this work will be documented at a later date.

APPENDIX I
SOLAR COLLECTION

Presented here is the derivation of Eqs. (3)-(5) for calculating the solar radiation energy abosrbed by the plastic layer, pond water, and steel deck when no evaporative layer is present. For the configuration where an evaporative layer is present a similar procedure will lead to Eqs. (8)-(11).

Consider solar radiation of horizontal surface intensity H_0 striking the surface 0 of the plastic membrane at incident angle θ_i, Fig. I.1. The angle of incidence on a horizontal surface for the beam radiation is given by [16]:

$$\cos\theta_i = \sin\phi\,\sin\delta + \cos\phi\,\cos\delta\,\cos\omega \qquad (I.1)$$

where the declination angle δ is given by [17]

$$\delta = 23.45 \sin 360 \left(\frac{284 + n}{365}\right) \qquad (I.2)$$

and

ϕ = Latitude with north positive, degrees

ω = Local hour angle, at solar noon = 0, 1 hr = 15 degrees

n = Number of the day, beginning with January 1

The incident rays are refracted according to Snell's law. It is assumed that multiple reflection is significant only within the plastic layer and the following fluxes are defined:

HT01 = Radiant energy transmitted through surface 0

HR01 = Radiant energy reflected from surface 0 toward surface 1

HR10 = Radiant energy reflected from surface 1 toward surface 0

HT12 = Radiant energy transmitted through surface 1

Using Eq. (1) in section II.1.1.1 for the radiation intensity at a distance X into the plastic and performing an energy balance one obtains the following set of equations:

$$HT01 = (1 - \rho_{ap})H_0 \tag{I.3}$$

$$HR01 = \rho_{ap} g_p \; HR10 \tag{I.4}$$

$$HR10 = \rho_{pw} g_p (HR01 + HT01) \tag{I.5}$$

$$HT12 = (1 - \rho_{pw}) g_p (HR01 + HT01) \tag{I.6}$$

where

$$g_p = e^{-\mu_p d_{pc}} = e^{-\mu_p d_{pc}/\cos\theta_p} \tag{I.7}$$

and θ_p = refraction angle at the air-plastic interface.

Equations (I.3)-(I.6) can be solved simultaneously for HT01, HR01, HR10, and HT12. The resulting expressions can be substituted into the following equations, to arrive at Eqs. (3-5) of Section II.1.1.1:

$$E_P = (1 - g_p)(HT01 + HR01 + HR10) \tag{I.8}$$

$$E_W = \sum_{n=1}^{5} \eta_n (1 - g_{wn}) HT12 \tag{I.9}$$

$$E_S = \sum_{n=1}^{5} \eta_n g_{wn} \; HT12 \tag{I.10}$$

APPENDIX II
PROPERTIES OF WATER

An empirical expression for the density of water as a function of temperature is given by Ref. [30]; this expression is valid from $0^{o}C$ to $150^{o}C$;

$$\rho = \frac{a_0 + a_1 t + a_2 t^2 + a_3 t^3 + a_4 t^4 + a_5 t^5}{1 + bt} \qquad (II.1)$$

where
$a_0 = 999.8396$
$a_1 = 18.224944$
$a_2 = -7.922210 \times 10^{-3}$
$a_3 = -55.44846 \times 10^{-6}$
$a_4 = 149.7562 \times 10^{-9}$
$a_5 = -393.2952 \times 10^{-12}$
$b = 18.159725 \times 10^{-3}$

and ρ and t have units of $kg\text{-}m^{-3}$ and ^{o}C respectively. The volumetric expansion coefficient is found from

$$\beta = \rho \frac{d}{dt} \frac{1}{\rho} \qquad (II.2)$$

by using the above expression for ρ.

Viscosity and thermal conductivity data from Ref. [23] were used to generate simple empirical expressions that fit the data over the entire temperature range of interest. The expression developed for the viscosity of water reproduces the data to within 5% error from $0^{o}C$ to $100^{o}C$.

$$\mu = \frac{1.283}{(50 + t)^{1.68}} \qquad (II.3)$$

where t and μ have units of ^{o}C and $kg\ m^{-1} sec^{-1}$ respectively. A quadratic equation was developed which predicts the thermal conductivity of water to better than 4% error from $0^{o}C$ to $150^{o}C$;

$$K = a_0 + a_1 t + a_2 t^2 \qquad (II.4)$$

where
$a_0 = 0.588815$
$a_1 = 8.738876 \times 10^{-4}$
$a_2 = -3.84741 \times 10^{-7}$

and t is in ^{o}C and K is in W m^{-1} $^{o}C^{-1}$.

The heat capacity of water is taken to be 4.180 kJ kg^{-1} $^{o}C^{-1}$ over the entire temperature range experienced in the roof pond model.

APPENDIX III
CALCULATION PROCEDURE

The major steps in the hourly calculations performed in the model are described below for each of four major system configurations:

Case 1. Top Insulation Closed, No Evaporative Layer

(1) The temperature of the outer surface of the top insulation is calculated by writing a heat balance for this surface and performing an iterative solution. The heat balance components are

- radiation loss between the surface and sky;
- solar radiation absorbed by the surface (if any);
- convective-conductive heat transfer between the surface and ambient air;
- heat transfer from the bottom side.

The heat transfer from the bottom side of the top insulating panel is based on the temperature of the plastic calculated during the previous time step and on an overall heat transfer coefficient between the plastic and the outer surface of the top insulation. The overall heat transfer coefficient between the plastic and outer surface of the top insulation is simultaneously calculated in this step.

(2) Based on the temperatures of the plastic and the encased water determined during the previous time step, the heat transfer coefficient between plastic and water is determined next. Using this result the overall heat transfer coefficient between the outer surface of the top insulation and water is calculated from which the heat flow into the water from above is determined.

(3) Based on the temperature of the steel obtained in the previous time step, the heat transfer coefficient between the steel and water is calculated from which the heat flow into the water from the deck is determined.

(4) A heat balance calculation is then performed on the pond water to obtain the current water temperature. This calculation is performed for each 20 minute period of the simulation (see section II.3).

(5) The steel temperature is determined by performing a heat balance on this surface and solving the resulting equation using an iterative method. This temperature is based on the new water temperature calculated in step (4).

(6) Recalculate the heat flows into the water from above and below and repeat steps (4) to (6) two more times.

Case 2. Top Insulation Open, No Evaporative Layer

(1) The solar energy (if any) absorbed by plastic, pond water, and steel is calculated.

(2) The temperature of the plastic membrane is calculated by performing an energy balance for this element and using an iterative solution technique. The temperature of the water obtained in the previous time step is utilized in the energy balance. The heat transfer coefficient between the plastic and the water and hence the heat flow rate into water from above are simultaneously calculated in this step.

(3) In the case of solar radiation, the steel temperature is calculated based on the water temperature obatained from the previous time step. If no solar radiation is present, the temperature of the steel from the previous time step is assumed.

(4) The heat flow into the water from below is calculated from the steel temperature obtained in step (3).

(5) Same as step (4) of Case 1.

(6) The steel temperature, heat flow into water from below, plastic membrane temperature, heat flow into water from above are recalculated and steps (5) and (6) are repreated.

Case 3. Top Insulation Open, With an Evaporative Layer

(1) The solar energy absorbed by the evaporative layer, plastic, pond water, and steel (if solar radiation present) are calculated.

(2) The evaporative and the convective-conductive heat losses from the evaporative layer to the environment are calculated using the evaporative layer temperature calculated in the previous time step. The flow rate of make-up water is calculated and the heat required to bring it to the temperature of the

evaporative layer is determined. The radiation exchange between the evaporative layer and sky is also calculated.

(3) The plastic temperature is determined by solving a heat balance on the plastic using an iterative procedure based on the temperatures of the evaporative layer and pond water which were obtained in the previous time step. If no solar radiation is present, the plastic temperature is assumed to have its previous value. The plastic-evaporative layer and plastic-water heat transfer coefficients are evaluated from which the heat flow into the evaporative layer from below, and into the water from above are determined.

(4) Same as Step (3) in Case 2.

(5) Same as Step (4) in Case 2.

(6) Same as step (4) of Case 1.

(7) The evaporative layer temperature is calculated by performing a heat balance on this layer for time periods of 1/9th of an hour, (See section II.3).

(8) The evaporative, convective-conductive, and radiative heat losses from the evaporative layer, and the plastic temperature are then recalculated. The heat flows from the plastic surface into both the evaporative layer and into the encased water are calculated and steps (7) and (8) and repeated two more times.

(9) The steel temperature and hence the heqt flow into the pond water from the steel are recalculated and steps (6) through (9) are repeated two more times.

Case 4. <u>Top Insulation Closed, With an Evaporative Layer</u>

(1) The temperature of the outer surface of top insulation is calculated in a manner which is similar to step (1) of Case 1. In this case, however, the heat transfer from the bottom side to the outer insulation surface is based upon the previous temperature of the evaporative layer rather than on the temperature of the plastic. An overall heat transfer coefficient between the evaporative layer surface and outer surface of the top insulation is determined. The heat flow from the top side of the top insulation into the evaporative layer is simultaneously calculated in this step.

(2) Based on the temperatures from the previous time step, the heat flow rates into the water and evaporative layer from the plastic and that into the water from the steel are calculated.

(3),(4) - Same as steps (4) and (5) of Case 1.

(5) The evaporative layer temperature is calculated by performing a heat balance on the water in the layer.

(6) The steel temperature, the plastic temperature, and heat flow rates into the evaporative layer and pond water from both above and below are recalculated.

(7) Steps (3) to (6) are repeated five more times.

In all of the four cases described above, the heat flow into or out of the room is calculated whenever the steel temperature is evaluated. This is done by calculating an overall heat transfer coefficient between the steel and the room, considering the presence or absence of the bottom insulation.

APPENDIX IV:

STANDARD PARAMETERS FOR THE BASE CASE

Dimensions

Depth of pond water	20 cm
Depth of evaporative layer	3 cm
Size of water bags	1 m × 1 m
Thickness of top air gap	3 cm
Thickness of bottom air gap	3 cm
Length of top insulation	3 m
Length of bottom insulation	3 m
Thickness of top insulation	3 cm
Thickness of bottom insulation	3 cm
Thickness of plastic layer	0.1 cm

Properties

Absorptivity of outer surface of top insulation	0.2
Emissivity of outer surface of top insulation	0.2
Emissivity of inner surface of top insulation	1.0
Emissivity of outer and inner surfaces of bottom insulation	1.0
Thermal conductivity of top and bottom insulations	0.09 $kJ \cdot m^{-1} {}^{\circ}C^{-1} hr^{-1}$
Emissivity of plastic	0.85
Overall absorption (or extinction) coefficient of plastic	0.4 cm^{-1}
Refractive index of plastic	1.5

	Heating Months	Cooling Months
Atlanta, Georgia	1-4, 10-12	5-9
Phoenix, Arizona	1-3, 11-12	4-10
Sacramento, California	1-5, 10-12	6-9
Washington, D.C.	1-5, 10-12	6-9

NOMENCLATURE

C	cloud cover in tenths (0 to 1)
C_p	heat capacity, $kJ \cdot kg^{-1} {}^{\circ}C^{-1}$
d_{fc}	path length of radiation through evaporative layer, cm
d_{pc}	path length of radiation through plastic membrane, cm
d_{wc}	path length of radiation through pond water, cm
e_a	atmospheric water vapor pressure, millibards in Eq. (16) and atm in Eqs. (21) and (22)
e_f	saturated water vapor pressure at temperature T_f, atm
E_F	total solar radiation absorbed by the evaporative layer, $kJ \cdot m^{-2} hr^{-1}$
E_P	total solar radiation absorbed by the plastic membrane, $kJ \cdot m^{-2} hr^{-1}$
E_S	total solar radiation absorbed by the steel decking, $kJ \cdot m^{-2} hr^{-1}$
E_W	total solar radiation absorbed by the pond water, $kJ \cdot m^{-2} hr^{-1}$
g	gravity acceleration, $m \cdot hr^{-2}$
g_p, g_{wn}, g_{fn}	defined by Eqs. (6), (7), and (12), respectively
Gr	Grashof number, $\beta \rho^2 \Delta T L^3 g/\mu^2$, dimensionless
h_c	convection-conduction heat transfer coefficient, $kJ \cdot m^{-2} hr^{-1} {}^{\circ}C^{-1}$
H_0	horizontal surface intensity of radiation, $kJ \cdot m^{-2} hr^{-1}$
$H(0)$	intensity of radiation entering a medium, $kJ \cdot m^{-2} hr^{-1}$
$H(X)$	intensity of radiation transmitted through a medium for a path length of radiation X, $kJ \cdot m^{-2} hr^{-1}$
K	thermal conductivity, $kJ \cdot m^{-1} hr^{-1} {}^{\circ}C^{-1}$
L	characteristic length, m
n	number of the day, beginning with 1 January
Nu	Nusselt number, $h_c L/K$, dimensionless

P	atmospheric pressure adjusted for altitude, atm
Pr	Prandtl number, $C_p\mu/K$, dimensionless
Q_C	convection-conduction heat transfer rate, $kJ \cdot m^{-2}hr^{-1}$
Q_e	evaporative heat transfer rate, $kJ \cdot m^{-2}hr^{-1}$
Q_r	radiation heat exchange rate between the system outer surface and the sky, $kJ \cdot m^{-2}hr^{-1}$
Q_{rm}	radiative heat exchange rate between the steel or the bottom surface of the inner insulation and room, $kJ \cdot m^{-2}hr^{-1}$
Q_w	heat required to bring make-up water from T_m to T_f, $kJ \cdot m^{-2}hr^{-1}$
Ra	Rayleigh number, GrPr, dimensionless
t	temperature, °C
T_a	dry bulb ambient temperature, °K
T_{av}, T_{fv}	defined in Eqs. (20) and (21)
T_f	temperature of the evaporative layer, °K
T_i	temperature of the surface exposed to the sky, °K
T_I	temperature at hour I, °C
T_j	temperature of steel or bottom surface of the inner insulation, °K
T_m	temperature of make-up water, °K
T_{max}	monthly average maximum temperature, °C
T_{min}	monthly average minimum temperature, °C
T_r	room air temperature, °K
T_{sky}	effective radiative sky temperature, Eq. (14), °K
V_w	volumetric flow rate of make-up water, $\ell \cdot m^{-1}hr^{-1}$
W	wind speed, $km \cdot hr^{-1}$
X	path length of radiation through a medium, cm

Greek Symbols

α	absorptance coefficient
β	volumetric expansion coefficient, °C^{-1}
δ	solar declination angle, degrees
ε_i	emissivity of the surface exposed to the sky
ε_{sc}	clear sky emissivity, Eq. (16)
ε_{se}	effective sky emissivity, Eq. (15)
η_n	fraction of solar radiation having absorption coefficient μ_n
θ_i	solar beam angle of incidence, degrees
μ	viscosity, $kg{\cdot}m^{-2}hr^{-1}$
μ_m	absorption (or extinction) coefficient of a medium, cm^{-1}
μ_n	absorption (or extinction) coefficient of water for the nth portion of the solar spectrum, cm^{-1}
μ_p	overall absorption (or extinction) coefficient of plastic, cm^{-1}
ρ	density, $kg{\cdot}m^{-3}$
ρ_{ap}	reflectance at the air-plastic interface
ρ_{aw}	reflectance at the air-water interface
ρ_{pw}	reflectance at the plastic-water interface
σ	Stefan-Boltzmann constant, $kJ{\cdot}m^{-2}hr^{-1}{}^{\circ}K^{-4}$
τ	coefficient of transmission = 1 - reflectance
ϕ	latitude with North positive, degrees
ω	local hour angle, at solar noon = 0, 1 hr = 15 degrees

REFERENCES

(1) H.R. Hay and J.I. Yellot, "Natural Air Conditioning With Roof Ponds and Movable Insulation," ASHRAE Trans., 75, Part I, 165-177 (1969).

(2) H.R. Hay and J.I. Yellot, "A Naturally Air Conditioned Building," Mech. Engrg., 92 (1), 19-23 (1970).

(3) H.R. Hay and J.I. Yellot, "International Aspects of Air Conditioning With Movable Insulation," Solar Energy, 12, 427-438 (1969).

(4) J.I. Yellot, "Early Tests of the Skytherm System," Passive Solar Heating and Cooling Conference and Workshop Proceedings, Albuquerque, New Mexico, 18-19 May 1976.

(5) P.W. Niles, K.L. Haggard, and H.R. Hay, "Nocturnal Cooling and Solar Heating With Water Ponds and Movable Insulation," ASHRAE Trans. Part I, 793-807 (1976).

(6) P.W. Niles, "Thermal Evaluation of a House Using a Movable-Insulation Heating and Cooling System," Solar Energy, 18, 413-419 (1976).

(7) W.C. Miller and T.R. Mancini, "Numerical Simulation of a Solar Heated and Cooled House Using Roof Ponds and Movable Insulation," presented at the Solar World Conference AS/ISES, Orlando, Florida, June 1977.

(8) R.E. Fate and T.R. Mancini, "The Performance of a Roof-Pond Solar House", Proceedings of the 4th National Passive Solar Conference Kansas City, Missouri, 728-732 (1979).

(9) J.D. Balcomb, J.C. Hedstrom, S.W. Moore, and R.D. McFarland, "Results From a Passive Thermal Storage Roof On a Mobile/Modular Home In Los Alamos," Los Alamos Scientific Laboratory, LA-UR-79-2672 (1979).

(10) G. Clark, C. Allen, F. Loxsom, and C.H. Treat, "A Regional Assessment of Evaporative, Radiative and Convective Cooling Processes and Systems In the United States," Trinity University San Antonio, Texas, 3rd Annual Solar Heating and Cooling R&D Contractor's Meeting, Sept. 1978.

(11) V.A. Baum, A. Kakabaev, and O. Klyshchaeva, "Equation for Calculating Flooded Roofs and Experimental Verification," Geliotekhnika, 3, (4), 51-55 (1967).

(12) V.A. Baum, A. Kakabaev, and O. Klyshchaeva, "Effectiveness of Flooded Roofs in a Hot Dry Climate," Geliotekhnika, 4, (4), 48-52 (1968).

(13) F.C. Houghton, H.T. Olson, and C. Gutberlet, "Summer Cooling Load as Affected by Heat Gain Through Dry, Sprinkled and Water Covered Roofs," ASHVE Trans., 46, 231-245, (1940).

(14) A. Defant, Physical Oceanography, Vol. 1, Pergamon Press, p. 53, (1961).

(15) A. Rabl and C. Nielsen, "Solar Ponds For Space Heating," Solar Energy, 17, 1-12 (1975).

(16) P. Berdahl, D. Grether, M. Martin, and M. Wahlig, "California Solar Data Manual," Lawrence Berkeley Laboratory, U.C. Berkeley, prepared for California Energy Commission and the U.S. Department of Energy, 1978.

(17) P.I. Cooper, "The Absorption of Solar Radiation in Solar Stills," Solar Energy, 12 (3) 333-346, (1969).

(18) W. D. Sellers, Physical Climatology, The University of Chicago Press, Chicago, p. 53 (1965). Quart. J. Royal Meterol. Society, 58, 389-420 (1932).

(19) W.C. McAdams, Heat Transmission, 3rd ed., McGraw-Hill, New York (1954).

(20) P.S. Klotz, "Heating Requirements of Swimming Pools," Engineering Thesis, Department Aeronautics and Astraonautics, Stanford University (1977).

(21) P.J. Ryan and D.R.F. Harleman, "An Analytical and Experimental Study of Transient Cooling Pond Behavior," Report No. 161, Ralph Parsons Laboratory for Water Resources and Hydrodynamics, Massachusetts Institute of Technology (1973).

(22) G.H. Jirka, M. Watanabe, K.H. Octavio, C.F. Cerco, and D.R.F. Harleman, "Mathematical Predictive Models For Cooling Ponds and Lakes, Part A: Model Development and Design Considerations", Report No. 238, Ralph Parsons Laboratory for Water Resources and Hydrodynamics, Massachusetts Institute of Technology (1978).

(23) J.P. Holman, Heat Transfer, 4th ed., McGraw-Hill, New York, (1976).

(24) ASHRAE Handbook of Fundamentals (1977).

(25) B. Gebhart, Heat Transfer, 2nd ed., McGraw-Hill, New Delhi, (1971).

(26) Climatic Atlas of The United States, U.S. Department of Commerce, Environmental Data Service (1977).

(27) B.Y.H. Liu and R.C. Jordan, "The Interrelationship and Characteristic Distributions of Direct, Diffuse, and Total Solar Radiation," Solar Energy, 4 (3), 1-19 (1960).

(28) J.A. Ruffner and F.E. Bair, The Weather Almanac, 2nd ed., Gale Research Co., 1977.

(29) Procedure for Determining Heating and Cooling Loads for Computerizing Energy Calculations, ASHRAE (1976).

(30) F. Franks, Water, A Comprehensive Treatise.

TECHNICAL INFORMATION DEPARTMENT
LAWRENCE BERKELEY LABORATORY
UNIVERSITY OF CALIFORNIA
BERKELEY, CALIFORNIA 94720